# RESIDUAL STRESS ANALYSIS OF HEAT-TREATED AlSi11Mg ALLOY WHEELS USING AN ANALYTICAL APPROACH

**Onur Özaydin and Aytaç Gören**
Mechanical Engineering Department, Dokuz Eylül University, İzmir, Türkiye

**Yiğit Çatal and Fulya Eyçin**
Design & PD Department, Döktaş Dökümcülük Tic. ve San. A.S., Manisa, Türkiye

Copyright © 2026 The Author(s)
https://doi.org/10.1007/s40962-026-01872-z

## Abstract

*This study investigates the microstructural evolution, mechanical performance, and residual stress distribution of AlSi11Mg alloy wheels produced by low-pressure die casting (LPDC) under various heat treatment conditions. Unlike conventional practice, where AlSi11Mg is often used without heat treatment, this work applied T6 and alternative heat treatments to assess their influence on critical wheel regions. Microstructural observations showed that the as-cast condition contained coarse dendrites and sharp Si particles, leading to low hardness and brittle behavior. Artificial aging alone produced limited precipitation hardening, whereas T6-treated samples exhibited refined and spheroidized Si morphologies, resulting in significantly higher yield strength, ultimate tensile strength, elongation, and hardness. Among the tested scenarios, Option #3 achieved the most balanced and consistent properties across all wheel regions. Residual stress simulations confirmed stress accumulation in hub and hub–spoke areas, a potential source of cracking. While T6 treatment maximized the strength, it also increased the residual stress; in contrast, limited heat treatments reduced the stress but compromised the mechanical performance. Complementary numerical simulations were conducted using Magmasoft and its Magmastress module to model both casting and heat treatment processes. Residual stress analyses highlighted that the highest residual stresses occur after quenching in T6-treated specimens. Long artificial aging time (Option #2) gives the lowest residual stress under T6-treated specimen groups. Stress relief annealing (Option #5) significantly reduced the residual stresses by 56–68%, reducing the risk of crack initiation. Overall, the study demonstrates that T6 heat treatment optimizes the mechanical performance in AlSi11Mg wheels, while stress relief annealing effectively decreases the residual stresses. These findings provide critical insights for the design, heat treatment, and quality assurance of aluminum alloy castings in automotive applications and potentially other thin-walled, complex components.*

Received: 24 October 2025 / Accepted: 23 December 2025
Published online: 11 February 2026

## Graphical Abstract

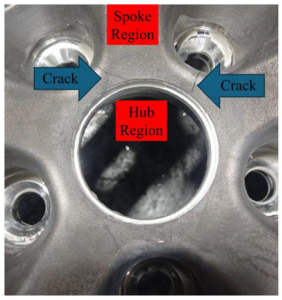


Suspected hub & hub/spoke area for cracks.

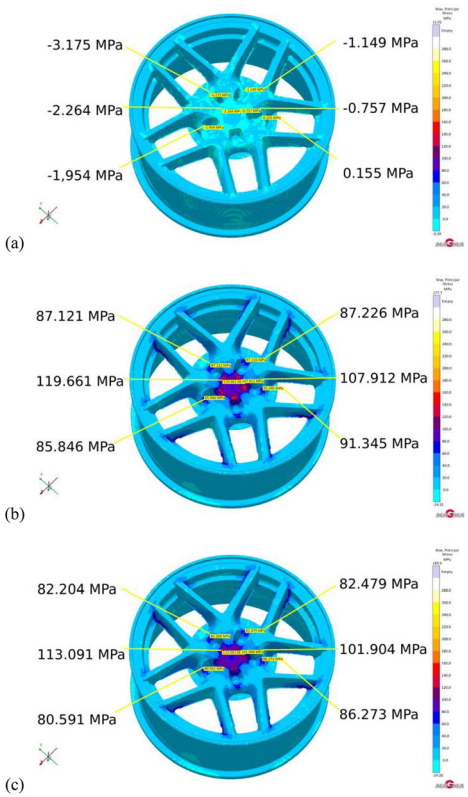


The results of Option #2 on various steps (a)After solution treatment, (b)After quenching, (c)After aging.

***Keywords:*** *AlSi11Mg alloy, low-pressure die casting (LPDC), heat treatment, residual stress, mechanical properties*

## Introduction

Although aluminum casting alloys are utilized in a wide range of fields such as aerospace, maritime, and defense industries, they are most preferred in the automotive industry compared to other sectors.[1] In recent years, the increasing demand for low carbon footprint and low emission values due to environmental concerns, combined with customer demand for reduced fuel consumption, has made the use of recyclable lightweight materials imperative in the automotive industry. European Aluminum research states that the production of recycled aluminum reduces $CO_2$ emissions significantly because it requires only 5% of the energy required to produce primary aluminum. Aluminum recycling rates in Europe are at 75%, while construction and vehicle recycling rates can be 90%.[2] The use of aluminum in the industry becomes increasingly

more important as the "Green Deal" seeks to reduce carbon emissions and carbon footprint.[3]

In the context of components used in the automotive industry, aluminum casting alloys are commonly preferred to produce critical parts such as cylinder blocks, cylinder heads, wheels, brackets, transmission components, and heat exchangers. Particularly for wheel applications, aluminum casting alloys offer significant advantages over alternative materials due to their high recyclability, lightness, and cost-effectiveness. When evaluated through Life Cycle Assessment (LCA), these properties make aluminum alloys a highly favorable choice. Considering the increasing environmental concerns, customer expectations, and the demand for sustainable products, aluminum casting alloys stand out as the most advantageous option for wheel production. From a metallurgical and mechanical standpoint, the ease of casting and machining, high corrosion resistance, excellent thermal conductivity, and the potential to enhance mechanical properties through heat treatment contribute to the widespread use of aluminum casting alloys.

Among all the aluminum casting alloys, AlSi7Mg and AlSi11Mg alloys are frequently preferred in aluminum alloy wheel production. In recent years, the demand for lighter yet mechanically stronger products has been steadily increasing, primarily driven by the need for improved fuel efficiency. To meet these demands, the application of additional processes to aluminum alloy cast components has become essential. Specifically for aluminum alloy wheels, heat treatment processes are employed to achieve the increasingly stringent requirements for high mechanical strength and toughness. For example, the T6 heat treatment process enhances tensile and yield strength, resulting in improved mechanical performance and increased toughness, which in turn leads to better results under fatigue and impact testing conditions.

However, despite these advantages, the high temperature gradients involved in the T6 process may lead to crack formation in critical regions of the product. These cracks can compromise the integrity of the component, especially when they appear in the form of micro- or macro-defects. While macrocracks can typically be detected through conventional inspection and testing methods, microcracks cause a more significant risk to product reliability, as they may propagate during service and cause delayed failures. Therefore, investigating the causes of crack formation due to thermal gradients during the heat treatment process is of vital importance.

In this study, it is evaluated that the cracks forming in the product after heat treatment steps involving high temperature gradients may be caused by residual stress within the material. Accordingly, the focus of the study is on the analysis of these residual stresses.

Residual stress can be defined as elastic stresses that form non-uniform within a material because of various manufacturing processes and/or heat treatment applications. Both mechanical and thermal effects play a significant role in the formation of residual stress. Mechanically induced residual stresses are associated with manufacturing processes such as machining, additive manufacturing, and welding. Thermally induced residual stresses arise from heat treatment procedures and thermal cycles. The most distinctive feature of residual stresses, which sets them apart from other types of stress, is their presence within the material in the absence of any external loads—whether mechanical or thermal.[4]

In this study, residual stress believed to be caused by thermally induced effects will be investigated. This investigation will begin with a review of residual stress measurement techniques, followed by the selection and application of the most appropriate measurement method based on the specific material and process involved.

Although the direct measurement of residual stress is not feasible, they can be determined indirectly through the measurement of deformation (strain) values. In industrial applications, depending on whether the component operates under tensile or compressive loads, residual stress within the material may cause risks such as compromising structural integrity or promoting crack propagation in the microstructure.[5,6] Moreover, the presence of tensile or compressive residual stresses in the component can cause the actual stresses experienced during service to differ from those calculated under nominal loading conditions. For instance, tensile residual stresses within the structure can reduce the service life of components subjected to fatigue loading by accelerating fatigue damage, whereas compressive residual stresses can enhance the service life under similar fatigue conditions. Additionally, depending on the design and manufacturing process of a component, tensile residual stresses may be present in one region while compressive residual stresses occur in another. Since the aluminum alloy wheel investigated in this study is an industrial application product subjected to tensile loading during fatigue tests, any potential compressive residual stresses act to inhibit or delay the opening and propagation of microcracks that may be induced by the tensile loads applied in the fatigue testing. Therefore, accurate and precise measurement of residual stress is of importance. Such measurements are crucial for component design, as well as for determining manufacturing and heat treatment parameters. Furthermore, since residual stress can also affect the dimensional accuracy of parts, their measurement becomes a critical step in industrial applications.

Various approaches can be observed in literature when classifying residual stress measurement methods. Some researchers categorize these methods as "destructive," "semi-destructive," and "non-destructive" measurement techniques,[4] while others classify semi-destructive methods under destructive measurement techniques.[7] In terms of the techniques included, destructive experimental methods include hole-drilling, ring-core, deep hole drilling, contour, layer removal (curvature), and sectioning techniques. Non-destructive experimental methods include X-ray diffraction (XRD), ultrasonic, neutron diffraction, and magnetic methods. Additionally, analytical methods involving residual stress measurement through analytical and finite element models are also considered.[7] Although classification schemes vary, analytical measurement methods, whose importance has grown in recent years, are evaluated as part of the "non-destructive" measurement category in both approaches. Due to the high setup costs and operational difficulties associated with destructive and semi-destructive methods, analytical and numerical modeling techniques offer significant advantages.

Among all Al-Si-Mg casting alloys, AlSi7Mg and AlSi11Mg alloys are frequently preferred to produce aluminum alloy wheels. Considering these two alloy types, AlSi7Mg offers certain advantages over AlSi11Mg in terms of heat treatability and is commonly referred to as the A356 (EN AC 42100) alloy.

Due to its high silicon content, the AlSi11Mg alloy, which contains a eutectic silicon phase in its microstructure, exhibits lower heat treatability compared to AlSi7Mg. The presence of insoluble eutectic silicon within the structure prevents it from contributing to precipitation hardening under T6 heat treatment conditions.[8] In AlSi11Mg alloys, the high silicon content leads to excessive formation of eutectic silicon, which diminishes the effectiveness of magnesium and silicon required for precipitation hardening.[9] The high silicon content in the microstructure creates a hard and brittle structure. This brittle microstructure limits the improvement of toughness and ductility values after heat treatment, preventing them from reaching the desired levels.

Despite the limitations of the T6 heat treatment applied to the AlSi11Mg alloy, its high castability has led to increasing industrial interest in heat-treated AlSi11Mg alloys in recent years. Moreover, the use of AlSi11Mg alloys is not limited to aluminum alloy wheels but extends to various automotive cast components, thereby enhancing the application potential of this alloy. Dahle et al. investigated the effect of grain refinement on fluidity in two aluminum casting alloys (AlSi7Mg and AlSi11Mg). In spiral mold tests, AlSi11Mg exhibited a longer spiral length, indicating better fluidity compared to AlSi7Mg. They attributed this to higher silicon content, which results in greater heat release and a tendency for dendrite fragmentation. Consequently, they noted that fluidity is influenced by multiple factors and concluded that the AlSi11Mg alloy provides improved mold-filling capacity during casting.[10]

According to the "Primary Aluminum Casting Alloys" report published by Rheinfelden Alloys, T6 and T5 heat treatments are applied to AlSi11Mg alloys. The T6 heat treatment process steps are listed as solution treatment (520–535 °C for 6–10 hours), water quenching (20 °C), and artificial aging (130–170 °C for 6–8 hours). The same report provides mechanical properties for as-cast and T6 heat-treated castings produced in permanent molds. According to these properties, for cast parts with a wall thickness up to 20 mm, improvements under T6 heat treatment compared to as-cast conditions are observed as follows: yield strength (YS) increased by 50%, tensile strength by 17%, hardness by 27%, and fatigue strength by 15%.[11]

## Heat Treatment

Aluminum-silicon alloys close to eutectic composition, such as the AlSi11 alloy, are preferred in the automotive and marine industries due to their high castability and low susceptibility to cracking. However, the irregular and sharp-edged eutectic silicon precipitates present in these alloys reduce impact resistance. The literature reports that soft annealing can refine and round these precipitates, thereby improving the material's plasticity. Jarco investigated the effects of soft annealing on the notch impact toughness (KC) and Brinell hardness (HB) of EN AC-AlSi11 (Al-Si alloy) material. The heat treatment was applied between 280 and 370 °C for durations ranging from 2 to 8 hours. The best results were obtained with annealing at 370 °C for 8 hours. While the annealing process increases plasticity (impact toughness), it decreases hardness. After annealing under ideal conditions (370 °C / 8 hours), impact toughness increased by 71%, whereas hardness decreased by 20% under the same conditions.[12]

Jarco and Pezda investigated the effects of T6 heat treatment (solution treatment followed by artificial aging) and its optimization on the mechanical properties and microstructure of Fe-containing AlSi11 alloy. Experimental studies conducted with different temperature and duration combinations revealed increases of 52% in tensile strength, 56% in elongation, 44% in hardness, and 88% in impact toughness. The heat treatment facilitated the spheroidization of eutectic silicon precipitates and homogenization of microstructure. The obtained data were analyzed using regression models to determine the optimal heat treatment parameters. Solution treatment temperatures between 510–545 °C and aging temperatures between 165–200 °C were identified as the most effective ranges.[13]

Vuksanović et al. reported a slight increase in strength and ductility, accompanied by a reduction in hardness, following the application of T6 heat treatment to the AlSi11 alloy. The treatment involved solutioning at 520 °C for 6 hours, followed by quenching in water at 70 °C. Subsequently, artificial aging was performed at 205 °C for 7 hours. After this thermal process, only a limited improvement in ultimate tensile strength (UTS) and elongation (%) was observed, while a noticeable decrease in hardness was recorded. These outcomes are primarily attributed to the limited magnesium content, the morphology of eutectic silicon, and the presence of detrimental intermetallic phases.[14]

Pedersen et al. applied heat treatment to four different AlSiMg foundry alloys, including Al-11Si-0.2Mg and Al-11Si-0.6Mg compositions. In the study, the T6 heat treatment involved three different solution treatment durations—1, 4, and 24 hours—at 540 °C. The quenching step was carried out in water, air, and oil at room temperature (25 °C), followed by artificial aging in oil at 150 °C for 4 hours. In the AlSi11Mg alloys, the ultimate tensile strength (UTS) increased primarily with magnesium content; the alloy with 0.6 wt% Mg exhibited the highest strength. However, even at this higher Mg level, extended solution treatment durations (240–1440 minutes) did not yield additional strength gains, as maximum strength was already achieved after 60 minutes. Ductility remained limited due to the high silicon content, with elongation (%) in AlSi11Mg alloys being significantly lower compared to AlSi7Mg alloys. During quenching, rapid cooling in water (average quenching rate: 97 K/s) led to higher strength, while slower cooling rates in air (1.8 K/s) and oil (12 K/s) reduced strength due to the formation of fewer $Mg_2Si$ precipitates. Although slower quenching can improve ductility, this effect is limited in high-silicon alloys like AlSi11.[15]

Abdelaziz et al. investigated the effects of various alloying additions and heat treatment on an AlSi11-based alloy. When comparing the effects of Mg and Cu additions, it was noted that a 0.4 wt% Mg addition resulted in a high ultimate tensile strength (UTS), comparable to that achieved with approximately 3 wt% Cu. The T6 heat treatment involved solutioning at 510 °C for 8 hours, quenching in water at 60 °C, and artificial aging for 5 hours at temperatures of 155, 180, 200, 220, and 240 °C. The highest strength values were obtained after artificial aging at 180 °C. The impact of the alloying additions in this study was observed as follows: Mg and Cu enhanced the strength via precipitation hardening, while Sr modified the silicon particles and improved the ductility. However, it was also noted that the combined use of Sr and Mg may reduce the modification efficiency, and the presence of intermetallic phases could act as potential sites for crack initiation.[16]

Altinel utilized Sr-modified AlSi11Mg as an aluminum alloy wheel material and investigated its properties under various testing conditions. The study determined the mechanical properties of samples aged at eight different temperature conditions ranging from 200 to −50 °C for specified durations. In the subsequent phase, samples were aged twice the duration at 150 and 0 °C based on previous study conditions, and the results were analyzed. The findings indicated no significant change in tensile strength at room temperature, while reductions were observed with increasing temperature. Yield strength exhibited the highest value at room temperature. Elongation values increased rapidly above 150 °C, whereas a slight decrease was observed below 0 °C.[17]

As stated above, due to the presence of insoluble eutectic silicon in AlSi11Mg alloy structures, the limited effect of the T6 heat treatment results in very scarce literature sources regarding industrial applications. Although this situation highlights the advantage and originality of this study in filling the gap in the literature, it also complicates referencing similar industrial studies. Therefore, AlSi10Mg casting alloys, which are widely used in the automotive industry and chemically very similar, were also examined. This approach provided significant insights for T6 heat-treated AlSi11Mg alloys.

Neuser et al. investigated the effect of solidification rates on the microstructure and mechanical properties of AlSi10Mg casting aluminum alloy, which is widely used in the automotive industry, under different thicknesses and heat treatment conditions to improve its mechanical performance. As-cast and T6 heat treatments were applied to AlSi10Mg plates with varying thicknesses (2–4 mm), and their mechanical properties (tensile strength, Brinell hardness) were examined. For thicknesses of 3 mm and above, it was concluded that increasing the solidification rate or enhancing the microstructure through modification elements is necessary.[18]

Mentese et al. conducted a study on the optimization of T6 heat treatment application for AlSi10Mg cast components used in industrial applications, specifically for engine bracket parts, considering variations in part dimensions and thicknesses. As a result of the optimized parameters, the study reported a 28% increase in total capacity and a 24% improvement in energy consumption.[19]

Beder et al. applied air cooling, quenching, and aging (T6 heat treatment) sequentially to die-cast AlSi10Mg alloy. The microstructures were examined using SEM and EDS, and it was observed that the structure gradually transformed into a more spheroidal form when subjected to heat treatments such as air cooling and quenching. After the T6 heat treatment, the yield strength (YS) of the cast AlSi10Mg increased by 70%, the ultimate tensile strength

(UTS) increased by 115%, and the wear resistance was also reported to have improved.[10]

## Residual Stress

In recent years, analytical measurement techniques have gained prominence due to their relatively low cost resulting from short setup and measurement times, as well as the absence of equipment and setup requirements. Advances in the finite element method (FEM) have also increased the reliability of obtained results.

Johnson et al. used the Magmastress software package to investigate the development of residual stresses during the casting process in a gray cast iron specimen. The sample parts were designed with a special geometry called the "Stress lattice" to induce residual stress within the component. Their simulations employed a thermo-elasto-plastic material model with temperature-dependent thermophysical properties. The simulation results were validated by comparing them with neutron diffraction measurements at different locations on the part.[20]

Menne et al. emphasized the importance of finite element modeling to predict the final mechanical properties, residual stress distribution, and potential defects in casting and heat treatment processes in some of Ford's R&D engine projects. The study concluded that finite element method modeling of the casting process as part of computer-aided engineering before engine block production could reduce time and costs by up to 50% and improve product quality and durability. Magmasoft software and various CAE tools were used for the analysis; however, details such as modeling parameters, boundary conditions, or material properties were not discussed in the report. Nevertheless, correlations were demonstrated by comparing analyses and real test results for different aluminum casting parts.[21]

Long et al. compared strain gauge measurements taken in a high-pressure die casting (HPDC) mold with a simulation model created using Magmasoft casting simulation software. Measurements taken throughout the casting cycle were compared to the von Mises stresses obtained from the simulation model. In this study, where two rosette strain gauges were used, differences of 10 and 40 MPa were observed between the experimental and simulation results at the relevant points. It was shown that the effects of additional factors that could not be simulated (such as mold clamping force and liquid metal pressure) on the mold were minimal.[22]

Jiang et al. investigated the effect of residual stress on the fatigue life of steel wheels. Residual stress formed on the surface during the rolling process of the steel wheel were simulated using ABAQUS software, and these values were compared with actual residual stress measurements taken from the surface. The simulation results showed good agreement between the regions of stress concentration predicted and those observed.[23]

Similarly to the study described above, He et al. modeled the solidification process of wheels using ProCAST. Distinctively, they transferred the SDAS calculation results into the ABAQUS model and developed a wheel fatigue model incorporating SDAS values. Based on the solidification (via ProCAST) and fatigue (via ABAQUS) analyses, they accurately predicted the fatigue damage region of the wheel and conducted an optimization study on the wheel mold and manufacturing process. Following the optimization, approximately a 37% reduction in SDAS values was observed, while increases in UTS and YS values were reported.[24]

Heger et al. analyzed residual stresses caused by non-uniform cooling due to varying wall thicknesses in heavy vehicle engines made of cast iron using Magmasoft and Magmastress modules. In recent years, they demonstrated improvements in predicting stress formation after material solidification, cooling, and heat treatment processes through software simulations by comparing different design variants with the original design.[25]

Li et al. investigated the parameters affecting the fatigue life of A356 automotive wheels in terms of residual stress, microstructure, and service conditions. Specifically, regarding residual stress, a model focused on the quenching step was developed. It was noted that the highest residual stresses occur in regions with the greatest temperature difference during quenching. According to the wheel model, approximately 90 MPa was observed in the spoke/hub area.[26]

Maijer et al. simulated the residual stresses of T6 heat-treated A356 automotive wheels and examined their effects on fatigue life. They compared the obtained analysis results with those from the sectioning technique. After heat treatment, they noted that the machining process reduced residual stress by 10 to 20%. However, they observed that the residual stress remaining on the surface after machining decreased the fatigue life.[27]

Cai et al. aimed to evaluate the residual stress developed in T4 and T6 heat-treated states of AlSi7Cu0.5Mg (A356) aluminum alloy. Analyses using different measurement techniques showed that the contour method and incremental hole drilling were most suitable for T6-treated alloys, while all methods were equally effective for T4-treated alloys. Additionally, they compared an analytical model with averaged surface displacement data, noting the greatest discrepancy in regions with macro-porosity.[28]

Özel et al. stated that it is difficult to precisely calculate residual stresses using analytical methods alone; therefore,

these methods are generally used in combination with experimental techniques to provide a good approximation, even if not exact. They also indicated that residual stress calculation can be performed using the numerical solution method of finite element analysis (FEA).[29]

Residual stress, besides being a phenomenon that can lead to fatigue damage, may itself constitute one of the root causes of fatigue failure, and it should be noted that various other root causes can also play a significant role in fatigue performance. Kreins et al. investigated the influence of shrinkage and hydrogen porosity on the fatigue life of the aluminum casting alloy AlSi11Mg and examined the crack initiation scenarios responsible for fatigue failure.[30] Hot tearing, which is one of the leading casting defects, should also be considered among the root causes that may lead to crack initiation, crack propagation, or structural damage.

## Materials and Methods

### Materials

Leading automotive manufacturers demand wheel products made from AlSi7Mg and AlSi11Mg alloys. These alloys are typically used as heat-treated AlSi7Mg and as-cast (non-heat-treated) AlSi11Mg. In this study, unlike other works, the use of AlSi11Mg material was preferred due to its ease of casting and high fluidity, as well as its potential applicability not only for wheel products but also for complex-structured engine parts. Contrary to traditional approaches, heat treatment was applied to the AlSi11Mg alloy, and alongside the noted improvements in mechanical properties reported in the literature, the effects of the high temperature gradients occurring during the heat treatment process on the structure and the causes of potential crack risks were examined. Thus, it is aimed to provide aluminum casting researchers with a new and different perspective by demonstrating the causes of possible risks and structural defects for a wider product range. From the material standpoint, chemical analyses and mechanical properties are primarily presented.

The chemical composition of the AlSi11Mg alloy and the mechanical properties at different production stages (as-cast without heat treatment and T6 heat-treated) are given in the tables below. It should be noted that the mechanical values represent minimum properties for parts cast in permanent molds with thicknesses up to 20 mm (Table 1).[11]

It should be emphasized that the values shown in Tables 1 and 2 are for primary aluminum casting alloys, as reported in the literature. Mechanical properties can vary depending on part and mold geometry, mold material, mold cooling conditions, casting process parameters, chemical composition, and heat treatment steps applied. All these factors will be standardized for each stage using sample values taken directly from the product. Samples taken from the product were prepared according to the DIN 50125 standard for tensile testing and tested according to the EN ISO 6892-1: 2016 standard. Tensile tests were carried out using Shimadzu AG-I 100 KN tensile testing machine in accordance with the relevant standards. Similarly, hardness measurements on the product cross-section were conducted using QNESS CS EVO 250 Brinell hardness tester following the ASTM E10 standard.

As with all studies involving industrial applications, reference values and limits will be presented and discussed under the "Results and Discussion" section according to the relevant standards and specifications that the industry refers to.

### Methods

Prior to wheel casting using the low-pressure die casting (LPDC) method, the feasibility of the casting process can be evaluated through numerical methods during the product verification stage. The analysis process in wheel casting begins with the creation of CAD models of the

***Table 2. Mechanical Properties of AlSi11Mg Aluminum Alloy[11]***

| Chemical composition | Yield strength [MPa] | Ultimate tensile strength [MPa] | Elongation [%] | Hardness Brinell [HB] |
|---|---|---|---|---|
| AlSi11Mg (as-cast) | 80 | 180 | 3 | 55 |
| AlSi11Mg (T6) | 120 | 210 | 3 | 70 |

***Table 1. Chemical Composition of AlSi11Mg Aluminum Alloy[11]***

| Chemical composition | Si | Fe | Cu | Mn | Mg | Zn | Ti |
|---|---|---|---|---|---|---|---|
| AlSi11Mg | 10.0–11.8 | 0.15 | 0.02 | 0.05 | 0.1–0.45 | 0.07 | 0.15 |

three primary mold components, namely the bottom die, top die, and side die. Subsequently, the remaining auxiliary components of the mold—such as the bottom plate, top plate, support columns, runners, cooling channels, and ejector pins—are modeled, and the product verification process proceeds accordingly. During this stage, a simulation is carried out by analyzing metal flow, mold filling, cooling, and solidification mechanisms. This enables both cost reduction and the implementation of necessary modifications or interventions prior to trial casting. These simulations can be performed using various software tools that employ different numerical approaches. For example: finite difference method (e.g., Magmasoft, FLOW-3D Cast, SolidCast), finite volume method (e.g., CastCAE, Noca-Solid&Flow), finite element method (e.g., CapCast, ProCAST), vector element method (e.g., AutoCAST).[31]

For the casting analyses in this study, the "Magmasoft Wheel" module—offered specifically to wheel manufacturers under the Magmasoft software that employs the finite difference method—was used.

In this module, as detailed above, the simulation begins with geometry definition, which is facilitated through a grouping approach during this stage. These groups may include the lower group, upper group, side molds, cooling systems, and cast parts. The mold components within each group are defined as either movable or stationary, and the movement axes and directions of the movable components are specified. Following the geometry definition, the material definition stage is carried out. After both the geometry and material definitions, the mesh generation process begins. In this stage—similarly to the finite element method—the mesh size must be sufficiently small to ensure accuracy close to experimental results, while also being coarse enough to maintain computational times within acceptable limits for serial production. Once the mesh has been generated, the definition stage follows, in which elements such as the casting material, lower-upper-side molds, runners, cooling systems, and air gaps are defined using the software's database, and their initial temperatures are assigned. To perform the heat transfer calculations, heat transfer coefficients are also specified at this stage. Finally, process parameters are defined. This includes mold filling, pressure filling, solidification, and cooling phases—all of which are configured in the software. Once the setup is complete, the simulation is run after selecting the parameters to be analyzed. Outputs such as metal flow velocity and turbulence during filling, temperature distributions of the part and mold during solidification and cooling, as well as porosity, can be selected and evaluated based on the simulation results.[32]

Heat treatment processes, like the low-pressure die casting method, can also be analyzed during the product validation phase. These analyses provide advantages both in evaluating existing heat treatment practices and in implementing alternative treatments at minimal cost. Just as in casting simulations, there are various software tools available that employ different approaches for simulating heat treatment processes. For example, integrated casting and heat treatment simulation software packages (e.g., ProCAST, Magmasoft) utilize Time-Temperature-Transformation (TTT) and/or Continuous Cooling Transformation (CCT) diagrams to simulate solid-state phase transformations and the development of mechanical properties during heat treatment.[31] Some software tools simulate the heat treatment behavior of aluminum alloys through Quench Factor Analysis (QFA) and by incorporating the Shercliff–Ashby model (e.g., SIMHEAT).[33] Additionally, simulation tools based on phase diagram calculations (e.g., Thermo-Calc and CALPHAD) based software can also be cited as examples.[34]

In this study, heat treatment simulations were carried out using the Magmasoft software. During the heat treatment steps, parameters such as furnace temperatures, process durations, process temperatures, and quenching media and their temperatures were defined within the software, allowing the simulation of heat treatment conditions. Through heat treatment simulation, it is possible to aim for the reduction of process times, evaluation of the effects of process variations on material properties, analysis of residual stress distribution, minimization of dimensional distortions, and overall reduction in costs.

In industrial products subjected to heat treatment, various methods exist for the measurement and calculation of residual stresses that may develop within the structure due to the very high temperature gradients during the process. Although different approaches are reported in the literature,[4,35–37] this study classifies these methods into destructive experimental techniques, non-destructive experimental techniques, and analytical techniques. Destructive experimental techniques include the hole-drilling method, ring-core method, deep hole-drilling method, contour method, layer removal/curvature method, and sectioning method. Non-destructive experimental techniques encompass X-ray diffraction (XRD), ultrasonic, neutron diffraction, and magnetic methods.

In this study, methods for analyzing residual stress using analytical and finite element models are classified as analytical techniques. Due to increasing costs related to measurement instruments, setup, and time in industrial applications, analytical and finite element models have been developed and increasingly adopted. The primary advantages of this approach are its relatively shorter processing times and the absence of costs associated with measurement devices and setup. However, its main disadvantage is the inability to fully replicate real conditions. One of the most significant advancements in analytical techniques is the development of finite element methods (FEM). This approach has greatly simplified the calibration

process of the critical stress relief coefficient, thereby improving measurement accuracy.[37]

Johnson et al. conducted a simulation study in Magmastress, based on a thermo-elasto-plastic formulation, as part of their benchmark analysis.[20]

The total strain, $\varepsilon_{Tot}$, is the sum of the mechanical and thermal strains, $\varepsilon_{Mech}$ and $\varepsilon_{Th}$, respectively, and is given by[20]

$$\varepsilon_{\{Tot\}} = \varepsilon_{\{Mech\}} + \varepsilon_{\{Th\}} = \varepsilon_{\{El\}} + \varepsilon_{\{Pl\}} + \varepsilon_{\{Th\}} \quad \text{Eqn. 1}$$

Thermal strain increments are calculated from the temperature history and integrated over time during cooling. The thermal strain also includes volumetric expansion and contraction from the phase transformations and is given by:[20]

$$\varepsilon_{\{Th\}} = \int_{T_1}^{T_2} \alpha(T) dT \quad \text{Eqn. 2}$$

where T and a are the temperature and thermal expansion coefficient, respectively.

Magmastress uses a well-known elasto-plastic formulation that is based on a combination of Hooke's law:[20]

$$\sigma_{ij} = \frac{E}{1+v}\left\{\varepsilon_{ij} + \frac{v}{1-2v}\delta_{ij}\varepsilon_{kk}\right\} - \delta_{ij}\frac{E\alpha\Delta T}{1-2v} \quad \text{Eqn. 3}$$

where $\delta_{ij}$ is the Kronecker delta, E is the Young's modulus, ν is the Poisson's ratio, and a classical formulation with a temperature-dependent yield condition including isotropic hardening is given by[20]

$$\varepsilon_{Mech} = \begin{cases} \frac{\sigma}{E} & for\ \sigma < \sigma_y \\ \frac{\sigma_y}{E}\left[\frac{1}{n}\left(\frac{\sigma}{\sigma_y}\right)^{\frac{\sigma}{E}} - \frac{1}{n} + 1\right] & for\ \sigma \geq \sigma_y \end{cases} \quad \text{Eqn. 4}$$

where n is the hardening parameter and $\sigma_y$ is the yield stress.

## Experimental Study: Numerical Study and Simulations

The trial production process begins with the melting of primary aluminum ingots and a certain amount of secondary aluminum in the melting furnace. During the melting process, master alloys AlSr15 (as modifier, 250 ppm) and AlTi5B (as grain refiner, 100 ppm) are added in specific proportions for grain refinement and modification, enabling the achievement of the desired chemical composition and microstructure. In order to remove dissolved hydrogen and possible inclusions from the melt, a degassing process is carried out by injecting inert gas into the liquid metal. Following this, the clean and prepared melt is transferred via ladles to the holding furnace of the low-pressure die casting machine, where it is held ready for casting.

In this stage of the study, the practical implementation of the previously described material and method information is examined. As a first step, the chemical composition of the AlSi11Mg alloy used in the experimental study is determined. The chemical analysis is carried out using an Optical Emission Spectrometer (OES), in which an arc is generated on the sample surface, causing localized burning. Due to its rapid and accurate results, OES is widely used in the industry. To ensure reliability, at least three burns are performed on the sample. In this study, chemical composition analyses were conducted in the laboratories of "Döktaş Dökümcülük Tic. ve San. A.Ş." using an 8820 ARL brand spectrometer in accordance with related standards as ASTM E415, E1086, E1251, E2994 (Table 3).

Following the achievement of the appropriate chemical composition, the molten metal, held at 750 °C in a ready-to-cast state, was subjected to chemical analysis and then transferred to the casting process. After casting, the rough burrs on the AlSi11Mg alloy wheels were removed by machining, and various heat treatment procedures were subsequently applied. The trial-cast wheels underwent a solution treatment at 535±5 °C in 200 minutes. Quenching was carried out in moderately stirred water at 80±5 °C in 70 seconds. At the final stage, artificial aging was applied at 155±5 °C in 150 minutes. In addition to this standard heat treatment process, alternative heat treatment routes specific to this study were also applied to evaluate their effects on mechanical properties and hardness values. Furthermore, all these process variants were simulated

***Table 3. Chemical Analysis of AlSi11Mg Aluminum Alloy***

| Chemical composition | Si | Fe | Cu | Mn | Mg | Zn | Ti | Sr | Al |
|---|---|---|---|---|---|---|---|---|---|
| AlSi11Mg | 10.81 | 0.12 | 0.01 | 0.00 | 0.15 | 0.03 | 0.11 | 0.03 | 88.74 |

analytically, and the effects of different heat treatment options on residual stresses were calculated using Magmasoft (Version 6.1) software.

During the experimental phase of the study, the mechanical properties and hardness values of the samples were measured separately before and after heat treatment. These measurements serve both to experimentally determine the material's mechanical performance and to investigate potential correlations with analytically calculated residual stresses. Regarding this correlation, Robinson and Redington used X-ray diffraction (XRD) to measure near-surface residual stresses and attempted to relate these values to the strength and hardness characteristics of heat-treated aluminum alloys.[38] They observed that for all examined aluminum alloys, the residual stress distribution through the thickness followed a similar pattern—tensile stresses developed in the interior regions, while compressive stresses occurred at the surface. The influence of alloy strength was reflected in the magnitude of the observed residual stresses. Moreover, a linear correlation was identified between surface residual stresses and both Vickers hardness and tensile strength after quenching.[38] Additionally, Wyatt et al. developed a low-cost method to determine surface residual stresses in cast components made from A356 aluminum alloy. By measuring the spacing variation between microhardness indentations, they calculated the stress levels and compared the mechanical and thermal stress relief techniques. The cast specimens were then subjected to thermal stress relief at 250 °C for 200 minutes, and the effectiveness of different stress relief methods was evaluated.[39]

Tensile tests were conducted in accordance with EN ISO 6892-1: 2016 standards using Shimadzu AG-I 100 KN tensile testing machine. The yield strength [MPa], ultimate tensile strength [MPa], and elongation [%] values were determined. Hardness measurements were performed in accordance with TS-139-1 standard, and the hardness values in the defined regions of the corresponding specimens were measured and summarized in the tables provided in the "Results and Discussion" section.

As detailed in the "Methods" section of this study, the simulation work begins with the definition of the low-pressure die casting (LPDC) process within the simulation software. In Magmasoft, the workflow follows a sequential structure consisting of the following modules: Project, Geometry, Mesh, Definition, (if applicable) Optimization, Simulation, Assessment, and Result. In the "Geometry" step, the mold and wheel model used in the study are defined using CAD files. In this stage, the material properties of all mold components and the wheel itself are assigned by utilizing the software's built-in material database. Additionally, the definition of movable components, such as the top and side dies (core slides), is also carried out in this step. Subsequently, an appropriate mesh structure is generated while simultaneously checking mesh quality. Special attention is paid to mesh size, density, and refinement in thin-walled regions to ensure accurate simulation results. Once the meshing is completed, the process proceeds to the "Definition" stage. Here, the casting alloy, lower/upper/side molds, runners, cooling channels, and air gaps are defined using data from the software's database. Initial temperatures for each component are also specified. To accurately model heat transfer, heat transfer coefficients are assigned in this step. These coefficients are defined for all contact interfaces between mold components in thermal interaction. Finally, the process parameters are defined. The stages of mold filling, pressure holding, solidification, and cooling are specified in detail and introduced into the simulation software (Figure 1).[40]

After all definitions are completed, the process advances to the simulation stage, where the simulation is executed to generate results for evaluation. In this way, the casting process of the wheel product is fully simulated using the Magmasoft Wheel module. Following the completion of the casting simulation, it becomes necessary to simulate the heat treatment process and calculate the resulting residual stresses. At this stage, the Magmasoft Stress module—a different module of the same software—is run. The primary objective of this module is to compute the stresses formed after casting and to accurately predict residual stress distributions. During the experimental production phase, once the wheel casting cycle is completed, the cast

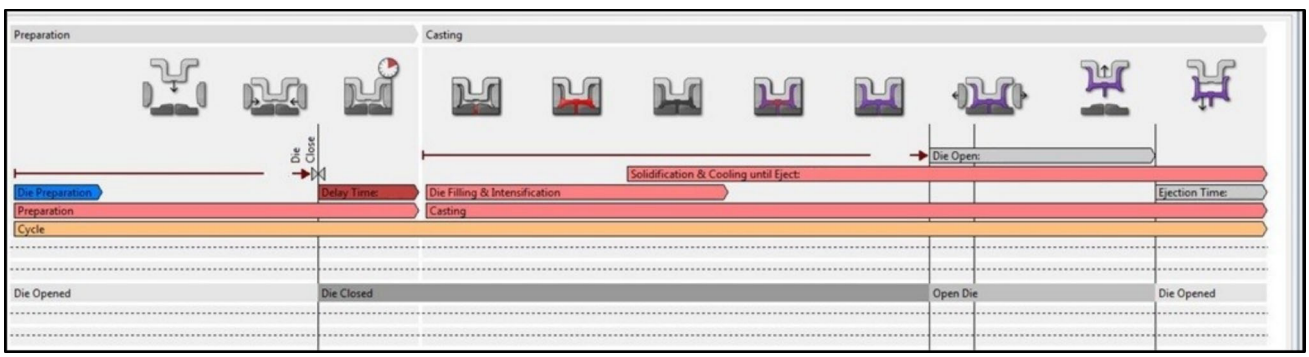


***Figure 1. Casting simulation process steps.*** [40]

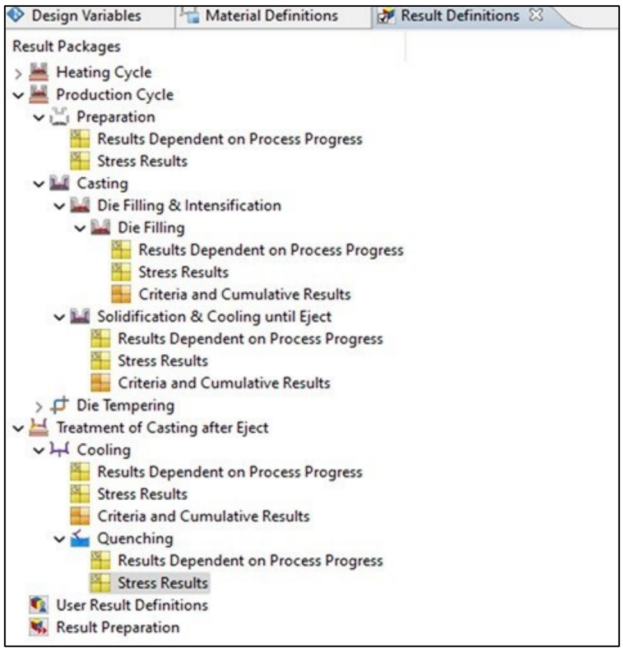


***Figure 2. Results definition in Magmasoft Stress module.***

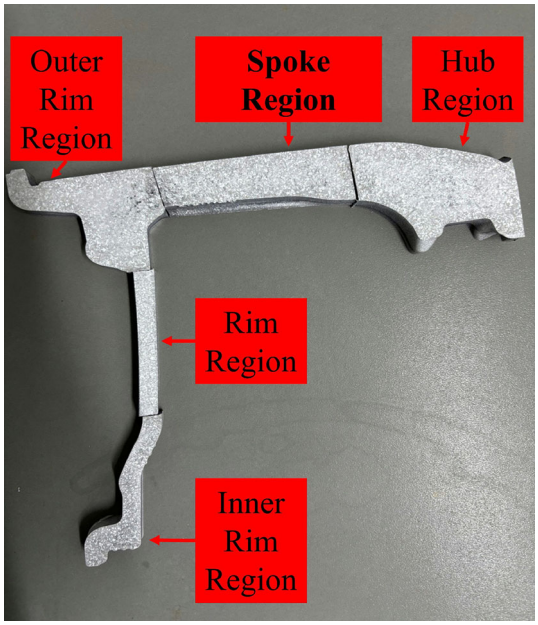


***Figure 3. Regions on the cross section of related wheel.***

wheel is removed from the die casting machine and transferred to a conveyor for X-ray inspection. During this handling process, the operator is responsible for performing necessary identification markings and for removing flash caused by mold parting lines. In order to safely perform this handling step, the wheel must first be partially cooled. For this purpose, it is immersed in water at 60 °C for 20 seconds to lower its temperature after casting. After being removed from the water and undergoing initial marking and rough flash removal, the wheel is placed on the conveyor belt for transfer to X-ray inspection. This handling process is required for all wheels, regardless of whether they undergo heat treatment, and must therefore be included in the simulation setup prior to the heat treatment simulation in order to ensure realistic and accurate simulation results.

Following the completion of the necessary steps related to the handling process, the heat treatment stages applied to the wheel product were also defined within the same module. In the Magmasoft Stress module, the procedure follows the sequence of geometry–material–meshing–solidification–boundary conditions–stress analysis–results evaluation–optimization, like the steps previously detailed. In this study, after defining the geometry, the materials for the casting, runner, stalk (riser), filter, and permanent mold components (top, side, and bottom cores) were selected from the material database embedded within the software. The mesh was generated such that at least three elements were present across the narrowest regions, and the relevant boundary conditions were defined accordingly. Distinct from the other modules, in the stress analysis stage (Figure 2), the "Results Definitions" section was extended to include the computation of "Stress Results." Consequently, the outcomes for the stages of Preparation, Die Filling, Solidification, and Treatment were presented.

During this definition phase, multiple alternative setups were created for specific purposes, and their outcomes are presented and discussed in the "Results and Discussion" section. In total, five different heat treatment scenarios were formulated prior to the heat treatment simulation:

The first scenario (Option #1) represents the commonly used as-cast condition for AlSi11Mg alloy wheels in the industry. In this case, only the handling-related definitions were included, while no heat treatment steps were assigned. As a result, relatively lower mechanical properties are expected compared to the other scenarios.

In the second (Option #2), third (Option #3) and fourth (Option #4) scenarios, a T6 heat treatment process was applied to the AlSi11Mg alloy, consistent with procedures used for other aluminum alloys. The steps defined in the simulation directly replicate those used by the industrial partner: solution treatment at 535±5 °C for 200 minutes, water quenching at 80±5 °C for 70 seconds, and artificial aging at 155±5 °C for 150 minutes. While higher residual stresses are expected in this scenario, the mechanical properties are also anticipated to be relatively high.

The fifth scenario (Option #5) addresses the concern of residual stress generation caused by the significant temperature difference during water quenching in the T6 treatment, which is frequently reported in the literature. To mitigate this effect, a treatment analogous to stress relief annealing was applied. This scenario aims to produce lower

*Table 4. Heat Treatment Process Parameters*

| | Solution treatment | | Quenching | | Artificial aging | |
|---|---|---|---|---|---|---|
| | temperature (°C) | Duration (min) | temperature (°C) | Duration (s) | temperature (°C) | Duration (min) |
| As-cast—Option #1 | N/A | N/A | N/A | N/A | N/A | N/A |
| Heat treatment—Option #2 | 535±5 | 200 | 80±5 | 70 | 155±5 | 150 |
| Heat treatment—Option #3 | 535±5 | 200 | 80±5 | 70 | 155±5 | 120 |
| Heat treatment—Option #4 | 535±5 | 200 | 80±5 | 70 | 155±5 | 90 |
| Heat treatment—Option #5 | N/A | N/A | N/A | N/A | 155±5 | 150 |

residual stresses, even though the mechanical properties are not expected to reach the levels of the T6-treated case.

## Results and Discussion

At this stage of the study, the findings are presented in three main parts: microstructural analyses, mechanical test results, and simulation outputs. The microstructural analyses focused on the effects of the as-cast condition and different heat treatment options, and the results were systematically compared. The results of these microstructural variations for the mechanical properties of the material were also discussed, with particular attention to the prediction of tensile strength and hardness. Subsequently, tensile and hardness tests were conducted on the critical regions of the wheel product, called as spoke, inner flange, and outer flange. To ensure statistical reliability, a minimum of three tests were performed for each case, and the results were summarized in the corresponding tables. Finally, the residual stress values and their distributions, calculated using the Magmastress module of the Magmasoft software for the defined processing options, were illustrated in the relevant figures. In this manner, the residual stresses induced by the selected production parameters were identified in terms of both values and distribution through an analytical approach.

### Microstructural Analysis

Table 5 shows microstructural images taken from the samples cut from the spoke region (Figure 3) for each option that is fixed in experimental study (Table 4) phases.

In the sample designated as Option #1 (as-cast condition) and presented in the table below, a distinctly dendritic solidification structure is observed, characterized by coarse and well-defined dendrite arms. This morphology is typically associated with high porosity risks, segregation, and structural heterogeneity. Consequently, relatively low mechanical performance, particularly in terms of tensile strength, is expected. Moreover, it should be noted that such a dendritic structure increases the possibility of crack initiation and contributes to brittle fracture behavior.

In Options #2, #3, and #4, the dendritic structure was significantly modified, resulting in a more spheroidized microstructure. The Si particles, influenced by the heat treatment, were refined and exhibited a relatively spheroidized morphology. At higher magnifications, these Si structures can be observed more clearly. The partial dissolution of Si during the solution treatment step, followed by the fine and dispersed precipitation during the aging step, contributed to the formation of this microstructure. Consequently, higher tensile strength and hardness values are expected compared to the as-cast condition. In Al-Si-Mg alloys subjected to T6 heat treatment, both hardness and tensile strength are expected to be considerably higher than those of the as-cast and short heat treatment (stress relief annealing) conditions. Among Options #2, #3, and #4, where differences are limited only to the artificial aging step of the T6 process, the microstructural analyses revealed significant similarities. Accordingly, no significant differences in tensile strength or hardness values are expected among these options.

In Option #5, the dendritic morphology closely looks like that of the as-cast condition, with coarse and sharp dendrite arms and a relatively coarse eutectic Si morphology. Unlike Option #1, some degree of precipitation hardening may have occurred; however, microstructural heterogeneity remains obvious. As a result, the mechanical performance is expected to be lower in terms of tensile strength and hardness when compared with the homogeneous structures obtained after T6 heat treatment, yet higher to that of the as-cast samples.

The microstructures of all options were obtained from samples taken from the inner rim (inner flange) region (Figure 3).

***Table 5. Microstructures of all Options***

| | X50 (Scale: 500µm) | X100 (Scale: 200µm) | X200 (Scale: 100µm) |
|---|---|---|---|
| As Cast Option #1 | 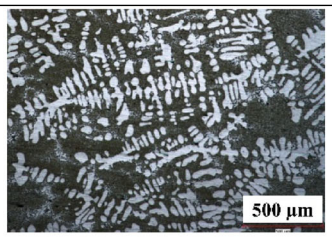  | 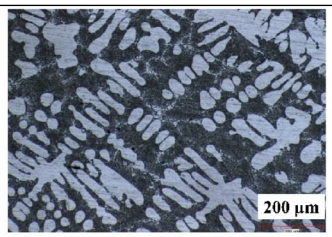  | 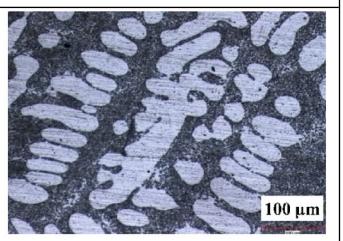  |
| Heat Treatment – Option #2 | 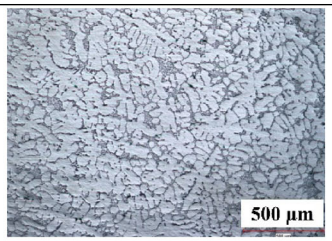  | 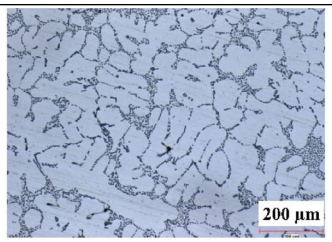  | 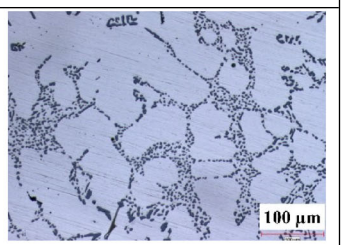  |
| Heat Treatment – Option #3 | 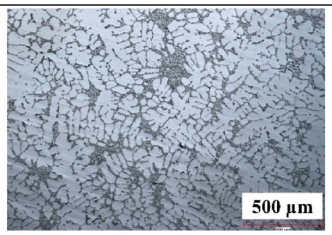  | 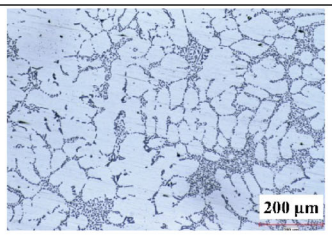  | 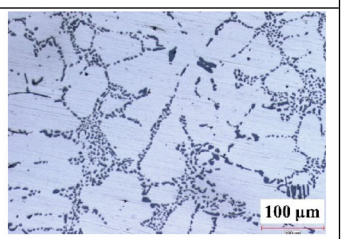  |
| Heat Treatment – Option #4 | 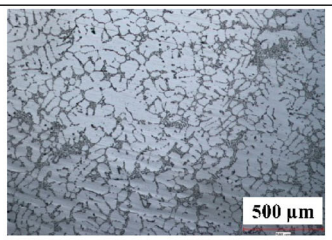  | 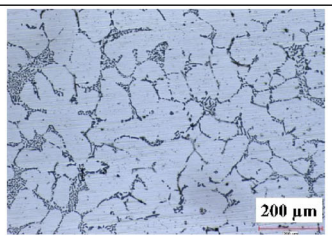  | 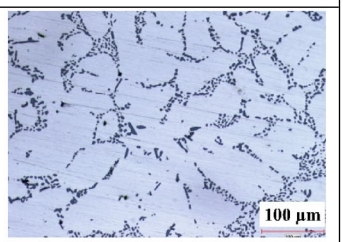  |
| Heat Treatment – Option #5 | 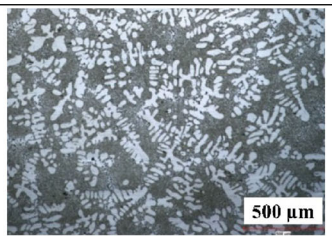  | 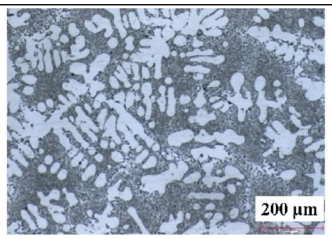  | 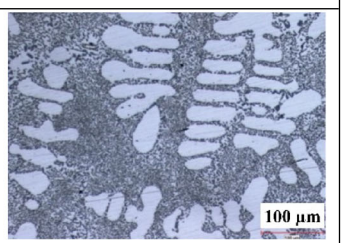  |

When the microstructures in Table 5 are compared, Option #1 exhibits the most heterogeneous morphology, characterized by coarse dendrites and sharp-edged Si particles, which are expected to result in low strength, reduced tensile and hardness values, and the most brittle behavior. In contrast, Options #2, #3, and #4 demonstrate the most homogeneous microstructures due to dendrite dissolution and Si spheroidization, thereby providing optimum tensile strength and hardness values. The variations in artificial aging duration among these three options did not lead to significant microstructural differences; however, it may be derived that extended aging (Option #2, 150 min.) could further promote Si spheroidization in critical regions (e.g., the spoke), thereby potentially providing slightly higher tensile properties. Finally, Option #5, which is similar to the as-cast structure (Option #1), is not expected to achieve the same tensile strength and hardness levels as the T6-treated samples. Nevertheless, owing to partial precipitation hardening, its mechanical properties are awaited to exceed those of the as-cast (Option #1) condition. For all

*Table 6. Mechanical Properties of AlSi11Mg Aluminum Alloy on Different Areas*

| | | Yield strength [MPa] | Ultimate tensile strength [MPa] | Elongation [%] | Hardness Brinell [HB] |
|---|---|---|---|---|---|
| As-cast—Option #1 | Inner Flange | 114.80 ± 0.1 | 199.80 ± 2.66 | 7.92 ± 0.35 | 56.45 ± 0.8 |
| | Outer Flange | 115.27 ± 0.33 | 202.38 ± 4.66 | 9.50 ± 0.97 | 55.95 ± 0.25 |
| | Spoke | 115.02 ± 2.11 | 170.01 ±1.39 | 3.24 ± 0.35 | 55.8 ± 0.55 |
| Heat treatment—Option #2 | Inner Flange | 192.57 ± 7.03 | 275.34 ± 11.79 | 13.95 ± 3.88 | 81.4 ± 0.8 |
| | Outer Flange | 191.15 ± 4.05 | 267.41 ± 23.43 | 11.78 ± 6.16 | 81.4 ± 0.1 |
| | Spoke | 170.86 ± 27.32 | 216.0 ± 27.85 | 3.67 ± 2.22 | 73.35 ± 0.05 |
| Heat treatment—Option #3 | Inner Flange | 190.70 ± 5.71 | 274.08 ± 8.78 | 14.56 ± 2.29 | 85.95 ± 0.75 |
| | Outer Flange | 188.58 ± 4.83 | 267.34 ± 8.97 | 13.33 ± 4.48 | 83.65 ± 1.85 |
| | Spoke | 166.96 ± 5.78 | 211.09 ± 17.19 | 3.49 ± 1.84 | 82 ± 0.1 |
| Heat treatment—Option #4 | Inner Flange | 174.43 ± 11.19 | 258.85 ± 13.65 | 15.82 ± 1.22 | 83.15 ± 0.15 |
| | Outer Flange | 173.86 ± 10.56 | 255.42 ± 13.71 | 14.79 ± 4.59 | 81 ± 0.1 |
| | Spoke | 155.98 ± 11.65 | 204.49 ± 15.54 | 4.24 ± 1.26 | 73.85 ± 0.75 |
| Heat treatment—Option #5 | Inner Flange | 117.96 ± 1.53 | 202.12 ± 18.17 | 9.02 ± 4.35 | 59.2 ± 2.2 |
| | Outer Flange | 117.16 ± 0.94 | 210.36 ± 2.5 | 10.69 ± 1.04 | 58.55 ± 1.55 |
| | Spoke | 117.57 ± 1.33 | 188.26 ± 12.16 | 4.18 ± 1.36 | 61.3 ± 0.7 |

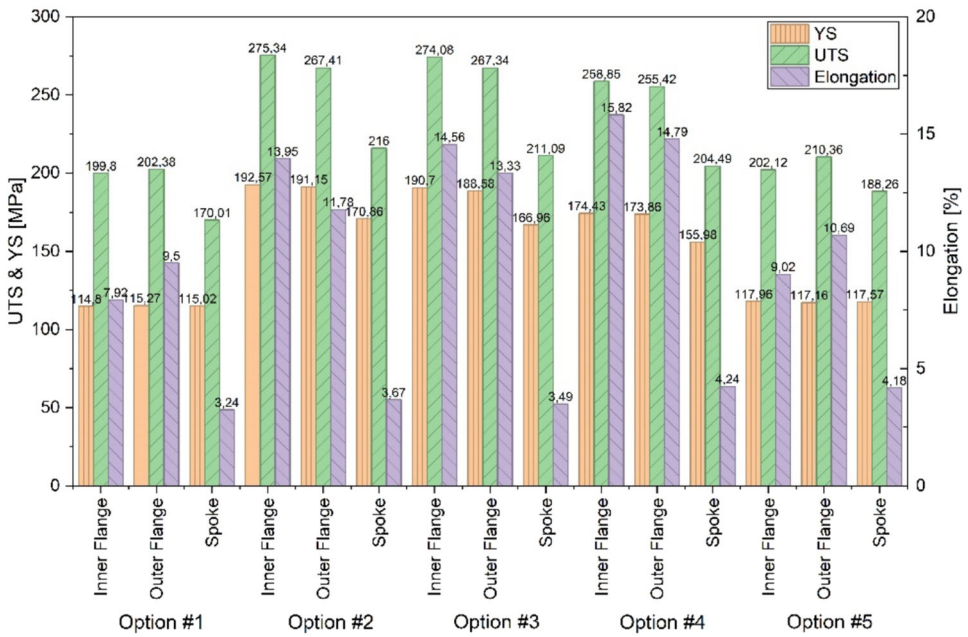


*Figure 4. Results of UTS [MPa], YS [MPa] and Elongation [%].*

options, SDAS measurements were conducted by taking seven measurements within an area of 3 $mm^2$. For Option #1, the average SDAS value was 29.67 μm (standard deviation: 18.88 μm); for Option #2, 33.47 μm (standard deviation: 14.51 μm); for Option #3, 31.11 μm (standard deviation: 18.11 μm); for Option #4, 30.07 μm (standard deviation: 12.98 μm); and for Option #5, 29.97 μm (standard deviation: 18.51 μm). Grain size evaluation was performed by comparison with a table prepared by the AFS Thermal Analysis Committee in accordance with ASTM Procedure E112. Based on the comparison with images at X200 magnification in this table, the grain size values were assessed to be in the range of 4–5. SDAS measurements were taken using samples taken from the inner rim (inner flange) region (Figure 3). The standard deviation observed in the SDAS values may be attributed to several factors, including local cooling variations within the relatively small measurement area (3 $mm^2$), regional casting defects,

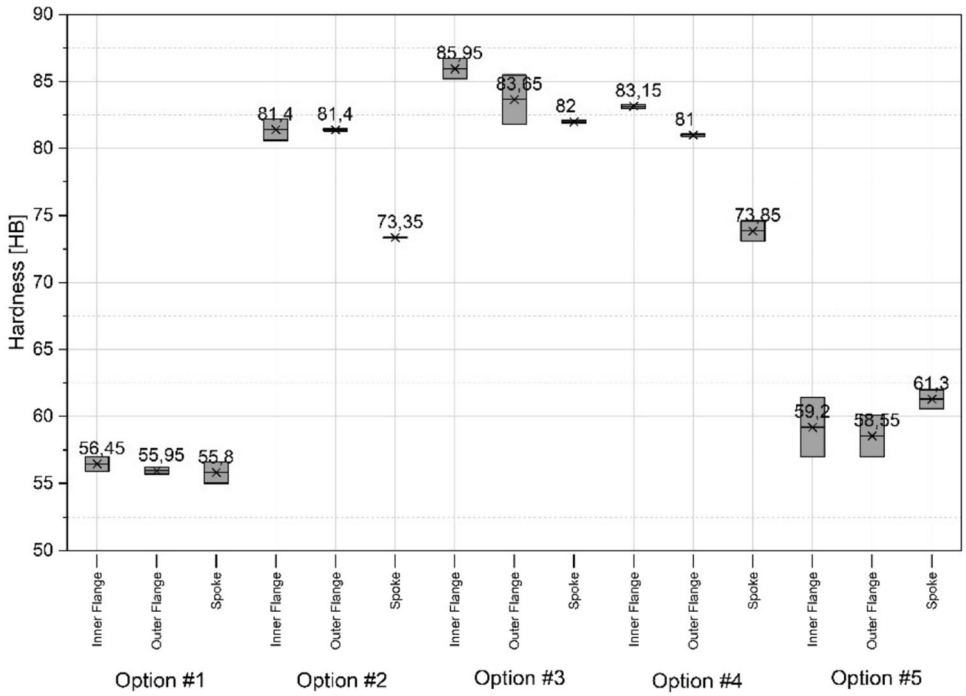


***Figure 5. Results of hardness Brinell [HB].***

and operator-dependent effects during the measurement process.

## Tensile and Hardness Properties

In this section of the study, the results obtained from the tensile and hardness tests performed on the specimens prepared in accordance with the previously mentioned standards are presented. Specifically, the tensile test results and hardness values for the three critical regions of the wheel product—inner flange, outer flange, and spoke—are summarized in Table 6 and illustrated in Figure 4.

Consistent with the expectations outlined in the previous section, the dendritic and heterogeneous microstructure observed in the non-heat-treated Option #1 specimens resulted in the lowest tensile test values compared to the other options. The brittle nature of this structure limited the achievement of higher ultimate tensile strength (UTS) and yield strength (YS). When the regional results of the wheel product are considered, the inner flange and outer flange exhibited similar values across almost all options, with the inner flange generally showing slightly higher UTS and YS. This behavior can be attributed to the fact that the inner flange is the first region to solidify during the low-pressure casting process. Since solidification proceeds sequentially through the inner flange, outer flange, and finally the spoke, the lowest UTS and YS values were consistently observed in the spoke region. A similar trend was observed for elongation, where the spoke region, being the last to solidify, exhibited dramatically lower values compared to the other regions. Regarding hardness, the highest values were obtained in the T6-treated Options #2, #3, and #4, while the lowest hardness was recorded in Option #1, which did not apply any heat treatment.

The hardness values are presented in detail in Figure 5. Among the samples, Option #1 exhibited the lowest hardness values across all three regions (inner flange, outer flange, and spoke), although no significant differences were observed between the regions. Similarly, in Option #5, which experienced a limited heat treatment (artificial aging only), a limited improvement in hardness was achieved through partial precipitation hardening. Comparable to Option #1, no significant change variation was observed among the different wheel regions. While the spoke, as the last solidifying region, would typically be expected to exhibit the lowest hardness, the differences among regions were insignificant, most likely due to the overall low hardness levels. When Options #1 and #5 are compared, Option #5 demonstrated a relatively small improvement of approximately 6% in the average hardness values of the defined wheel regions. This outcome consists of the mechanical strength results and fit with the expected performance.

Conversely, the T6 heat-treated Options #2, #3, and #4 exhibited an obvious improvement in hardness compared with Options #1 and #5. This outcome is consistent with the dissolved dendritic and homogeneous microstructures observed, which provide the results predictable. In Option #2, a marked increase was recorded particularly in the flange regions, with hardness values reaching up to 81.4

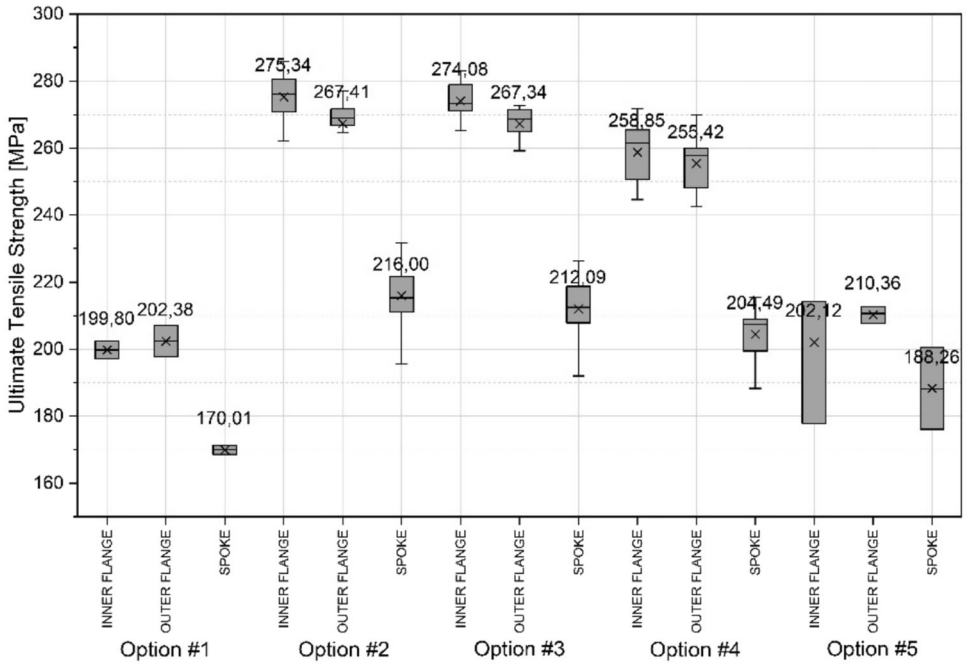


***Figure 6. Results of ultimate tensile strength (UTS) [MPa].***

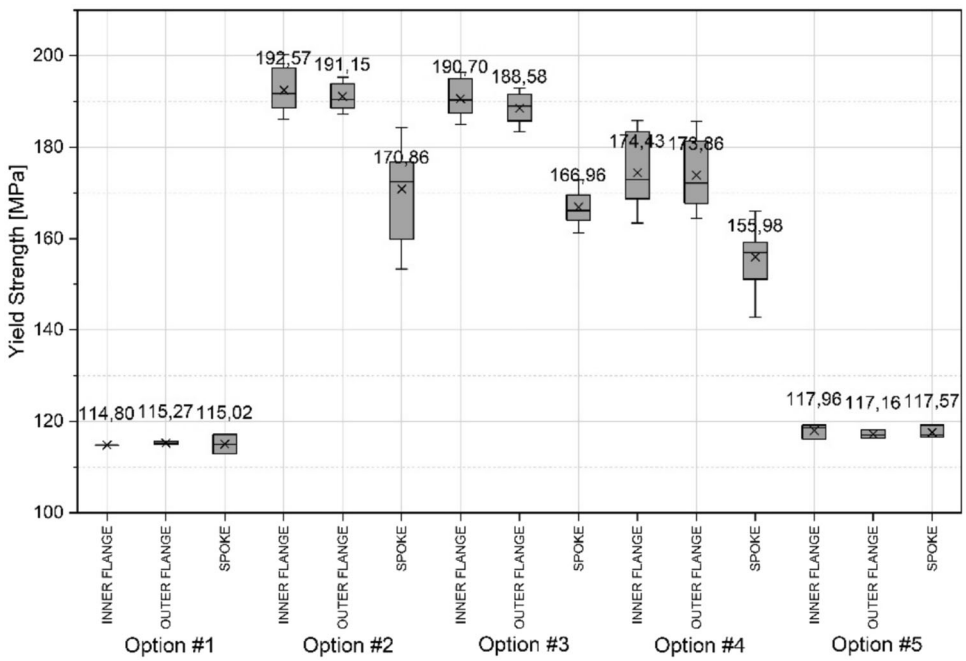


***Figure 7. Results of yield strength (YS) [MPa].***

HB; however, a lower value (73.35 HB) was observed in the spoke, likely due to its late solidification. A similar trend was clearly obvious in Option #4, whereas in Option #3, although a comparable trend was expected, the improvement was more uniform. Option #3 provided the highest hardness values among all conditions (inner flange: 85.95 HB, outer flange: 83.65 HB, spoke: 82 HB), indicating a more homogeneous distribution across regions. Option #5, while outperforming Option #1 due to limited precipitation hardening, remained well below the values obtained for Options #2, #3, and #4. Although Options #2 and #4 demonstrated high performance in specific regions, their lower hardness values in the spoke limited their overall structural consistency. By contrast, Option #3 was remarkable as the most advantageous condition, offering consistently high and balanced hardness across all regions. Nevertheless, when Options #2, #3, and #4 are compared with one another, the differences in average hardness

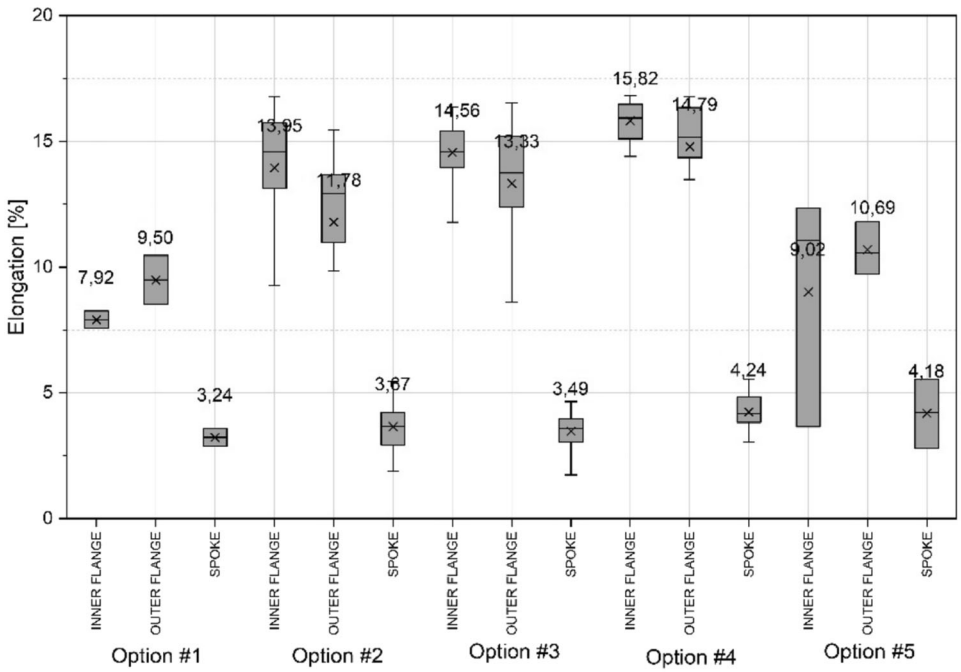


***Figure 8. Results of elongation [%].***

across the defined wheel regions were relatively minor, on the order of 5–6%. Finally, in comparison with the literature values (Table 2), the hardness values of Option #1 were found to be similar, whereas those of Options #2, #3, and #4 exceeded the reported ranges.

In the following figures (Figures 6, 7, 8), the ultimate tensile strength (UTS), yield strength (YS), and elongation (%) obtained from tensile testing are presented comparatively. It is obvious that the distinct heat-treatment applied in Options #1 through #5 produces noticeable effects on material properties.

A detailed examination of Figures 6, 7, 8—which, respectively, report UTS, YS, and elongation—shows that the T6-treated groups (Options #2, #3, and #4) deliver the highest UTS, YS, and elongation values relative to the remaining conditions. With respect to UTS and YS, Option #2 (longer artificial-aging time: 150 min) and Option #3 (intermediate artificial-aging time: 120 min) exhibit nearly indistinguishable results.

At this stage, when the prior hardness data are also considered, Option #3 appears as the most favorable among the alternatives. Within the T6-treated groups, Option #4 shows the lowest tensile outcomes (UTS and YS). Based on these findings, a minimum artificial-aging time of 120 minutes (as in Option #3) is recommended to achieve optimal combinations of mechanical properties and hardness. With a shorter artificial-aging time of 90 minutes (as in Option #4), UTS decreases of 5–6% and YS decreases of 7–9% were observed across different wheel locations. By contrast, extending the artificial-aging time to 150 minutes (Option #2) provides no meaningful improvement and results only in limited increases.

When the options are evaluated across different wheel regions (inner flange, outer flange, and spoke), the T6-treated specimens as expected show lower UTS and YS in the spoke—a region that cools later during the solidification sequence—than in the inner and outer flanges. A similar trend in UTS is observed for the non-heat-treated Option #1 and the artificially aged-only Option #5; however, for YS the regional differences under these two conditions remain quite limited.

In summary, before designating a single option as "optimal" product-level performance expectations and acceptable limits must be clearly defined. The present study demonstrates that these expectations may vary not only at the material properties but also locally across different regions of the wheel.

According to the results, where high UTS and YS are required—irrespective of the sampling region—the most suitable choices are Option #2 or Option #3. Nevertheless, among the T6-treated conditions (Options #2, #3, and #4), the extended artificial-aging time of Option #2 produces nearly no effect on UTS and YS in the inner and outer flanges (maximum differences of 0.45% for UTS and 1.34% for YS). Although the spoke exhibits more noticeable differences (1.8% for UTS and 2.28% for YS), these gains are not operationally convincing when manufacturing constraints are taken into account. In view of these facts, Option #3 can be identified as the preferred choice in applications that primarily demand high UTS and YS.

Conversely, where relatively high elongation is prioritized, Option #4 is the most suitable. Within the T6-treated set (Options #2, #3, and #4), Option #4 provides elongation values that exceed those of Option #2 (the lower-ductility condition) by 13–25% in the inner and outer flanges and by 16% in the spoke.

Across all comparisons, Option #5 (artificial aging only) outperforms the as-cast, non-heat-treated Option #1. However, when compared against the T6-treated options—particularly in terms of UTS and YS—Option #5 is clearly poor.

For nearly all options, the lowest UTS, YS, and elongation values occur in the spoke of a given option; in exceptional cases, any deviations are negligible. This finding emphasizes the importance of closely inspecting the spoke/hub region, where residual stress can develop. The consistently lower tensile results in this region, relative to the flanges, indicate that residual stress may compromise structural integrity and raise risk. Consequently, the need for residual-stress analyses and calculations—validated on representative specimens—is emphasized again.

## Simulation Results

In this section, the residual stress values obtained using the Magmastress module of the Magmasoft software for the different options involving various heat treatment applications are presented.

As detailed earlier in this study, the analytical method study began with the simulation of the wheel casting process using the low-pressure die casting (LPDC) method to verify the castability of the product. After confirming the castability of the wheel model, the analysis proceeded with the Magmastress module within the same software to calculate the residual stress values, which established the main objective of this study. Undoubtedly, using the wheel data obtained from the basic casting simulation—containing the effects of filling and solidification—is crucial for accurately demonstrating their influence on the final results. Otherwise, considering only the heat treatment effects in the Magmastress module would not represent the experimental casting process and would neglect the impact of the filling and solidification stages on the final stress distribution. Therefore, ensuring the accuracy and appropriateness of the input data provided to the Magmastress module is of critical importance for the reliability of the residual stress analysis.

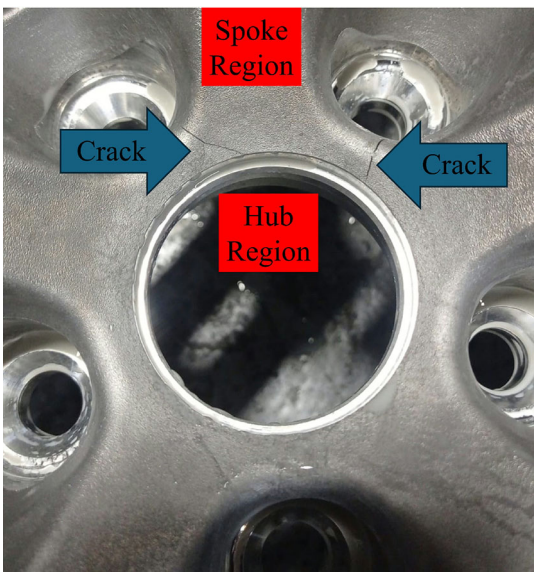


*Figure 9. Suspected hub and hub/spoke area for cracks.*

One of the key aspects that distinguishes this study from other examples in the literature—where only the filling and solidification stages and their effects during casting simulations are analyzed—and that provides originality to the work, is the concentration of residual stress analysis. Therefore, this section focuses on and presents the results obtained from the Magmastress module. Additionally, no external loads were applied to the wheel data used in the analytical studies. This approach allowed the residual stress values within the structure to be directly calculated through the software.

The different heat treatment procedures detailed in Table 4 were defined within the Magmastress module and applied to the wheel data obtained from the casting simulation. In this way, separate versions were generated for each option, and the corresponding results were analyzed and presented. In all analyses, attention was concentrated on the hub and hub–spoke regions (Figure 9), where cracking was also observed during experimental study, in order to ensure consistency between simulation and experimental production behavior.

Firstly, in Option #1, which represents the as-cast condition without any heat treatment, the handling process—defined as immersion in water at 60 °C for 20 seconds followed by

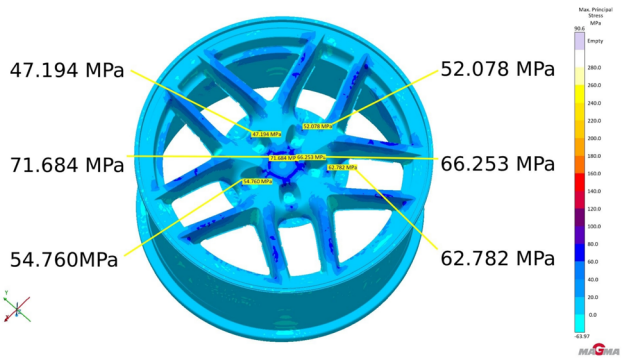


*Figure 10. The effect of handling process on residual stress (Option #1).*

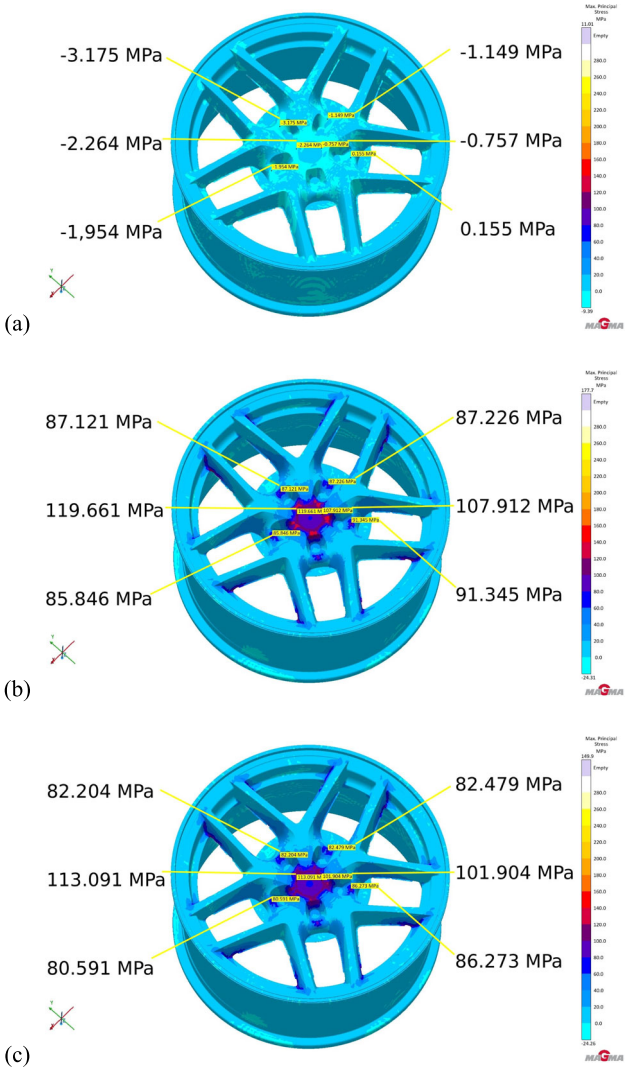


***Figure 11. The results of Option #2 on various steps: (a) after solution treatment, (b) after quenching, (c) after aging.***

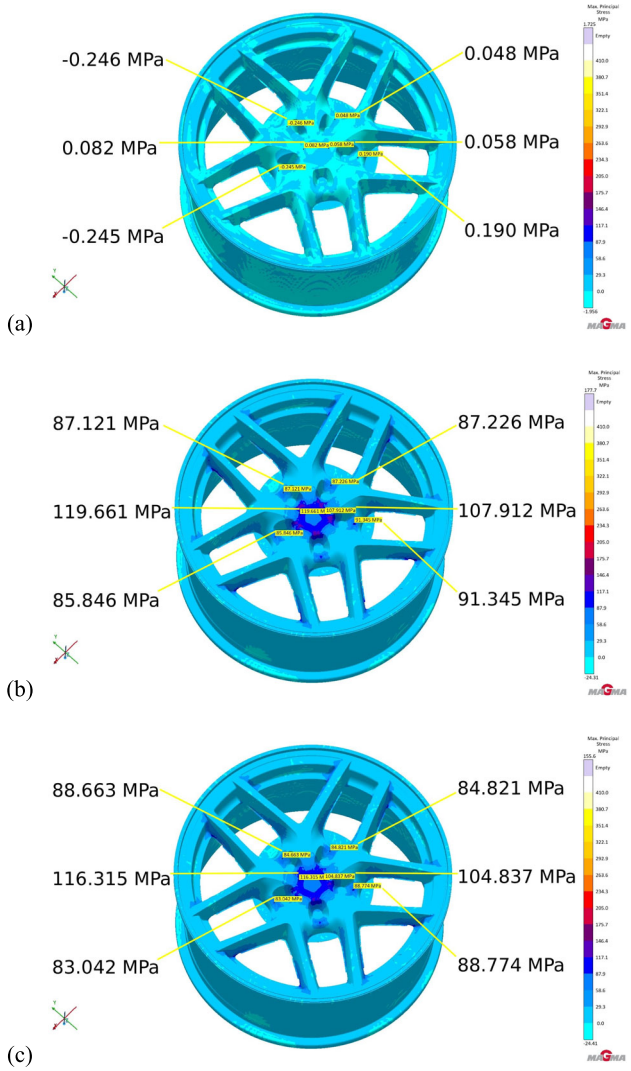


***Figure 12. The results of Option #4 on various steps: (a) after solution treatment, (b) after quenching, (c) after aging.***

air cooling—was integrated into the simulation to observe its potential effect, as detailed in Section "Experimental Study: Numerical Study and Simulations". Although, in industrial practice, the influence of this process on residual stresses is generally considered negligible—since it is expected to be eliminated during the following solution heat treatment step—its effects were nevertheless calculated and presented in this study using the software (Figure 10).

This analysis is also valid and significant for the other options that experienced heat treatment, since all of them share the same initial condition prior to heat treatment and immediately after the handling process. The residual stresses formed in the structure following the handling process were observed to range between 66–71 MPa in the hub region and 47–62 MPa from the hub toward the spoke region. Although these values are shown in later sections to vary under different heat treatment conditions (e.g., during the T6 process), they are important in establishing an understanding of the inherent residual stress present in the as-cast specimens (Option #1) before any heat treatment is applied.

In the second stage of the analysis, simulations were performed for the wheel products subjected to T6 heat treatment, including Options #2, #3, and #4, which differed in artificial aging durations (150 min, 120 min, and 90 min, respectively). In this analysis, the hub and hub–spoke regions—identified as critical areas with crack risk in the actual product (Figure 9)—were examined in detail. Within this T6-treated group, the specimens with the longest and shortest artificial aging durations, namely Option #2 and Option #4, were analyzed first. For these options, residual stress calculations were conducted not only after the complete process but also at all major stages of the T6 heat treatment (after solution treatment, after quenching, and after aging), thereby demonstrating the evolution of

residual stress throughout the process. Figure 11 presents the residual stress results obtained from the software for Option #2, which has the longest artificial aging duration.

The results presented in Figure 11 clearly indicate that, following the solution treatment step, the structure exhibited almost zero—and in some regions even compressive—residual stresses due to the high-temperature effect (Figure 11a). As expected, the highest tensile residual stresses were obtained after the quenching stage, where the temperature difference during heat treatment was at its maximum. In this step, the residual stresses ranged from 107–119 MPa in the hub region and from 85–91 MPa in the area extending from the hub toward the spoke region (Figure 11b). In the subsequent artificial aging stage, the expected relief of residual stresses due to the influence of temperature and time was confirmed by the obtained results: residual stress values ranged from 101–113 MPa in the hub region and from 80–86 MPa in the hub–spoke transition region (Figure 11c). When these values were compared with their corresponding points, an average stress relaxation of approximately 5.53% in the hub region and 5.69% in the hub–spoke region was observed.

The results for Option #4, simulated using the same approach, are presented in Figure 12.

For Option #4, which has the shortest artificial aging duration, the results detailed in Figure 12 closely are similar to Option #2. During the solution treatment step, almost negligible tensile residual stresses—and occasionally compressive residual stresses—were observed in the structure (Figure 12a). However, these values are too small to allow meaningful comparison or evaluation, and it can be stated that the residual stresses in both options (Option #2 and Option #4) are effectively neutralized at this stage. Following the quenching step, where the highest temperature differential occurs, identical results were obtained (Figure 12b), since no changes were made to the simulation parameters up to this step, despite separate versions run for this option. In the subsequent artificial aging stage, as expected, some stress relaxation was observed, with residual stress values ranging from 116–104 MPa in the hub region and 83–88 MPa in the hub–spoke region. When these values were compared point by point with their corresponding locations, average stress relaxation of approximately 2.82% in the hub region and 2.91% in the hub–spoke region was observed.

Finally, when comparing Options #2 and #4, the longer artificial aging duration of Option #2 (150 min) resulted in lower residual stresses compared to the shorter aging duration of Option #4 (90 min). The only difference between these two options lies in the variation of the aging time during the artificial aging step. In Option #2, which has the longer aging duration, residual stresses were reduced by approximately 2.78% in the hub region and 2.86% in the hub–spoke region compared to Option #4.

When evaluating all these values, it is evident that Options #2 and #4, both subjected to T6 heat treatment, produced almost same results up to the "After Quenching" step. In the case of the longer artificial aging duration (Option #2, 150 min), residual stress relaxation in the critical hub region exceeded 5.5%, whereas for the shorter aging duration (Option #4, 90 min), the relaxation was limited to approximately 2.8%.

Due to the minimal differences between Options #2 and #4, and the fact that all other simulation parameters—except for the artificial aging duration—remained same, it was expected that Option #3 would give intermediate values with only a negligible difference compared to these two options. Therefore, a separate analysis for Option #3 was considered unnecessary.

Based on all these analyses and observations, it can be concluded that, within the T6 heat-treated group, Option #2—with the longest artificial aging duration—exhibited the lowest residual stresses. Considering the residual stress risk, Option #2 can therefore be identified as the most suitable choice. The fundamental principle underlying the reduction of residual stresses with increasing aging time is dislocation movement, also referred to as dislocation relaxation/creep, or climb.

In the third and final stage of the analysis, the simulation was performed for Option #5, which experienced a heat treatment process without the solution treatment and quenching steps—commonly referred to in the literature as stress relief annealing[39]—in comparison with the T6 heat treatment. Since the quenching step was bypassed, the process avoided the high-temperature gradients that typically generate very high residual stresses. Nevertheless, as with all other options, Option #5 underwent the handling process, which is part of the production sequence. Consequently, prior to stress relief annealing, the residual stresses from the handling process, as shown in Figure 10, were

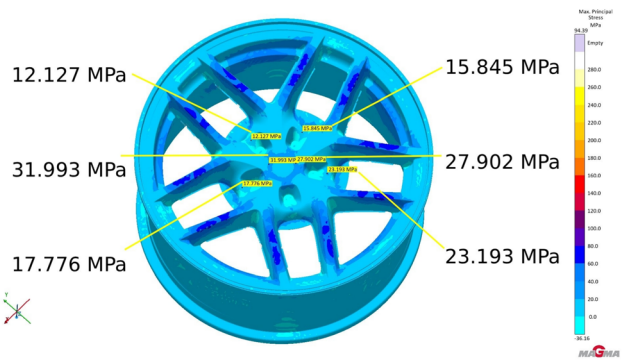


***Figure 13. The results of Option #5 after stress relief annealing.***

carried into the heat treatment step (155 ± 5 °C, 150 min), and the corresponding changes in residual stresses during this process are presented in Figure 13.

Following the stress relief annealing process, as detailed in Figure 13, the hub and hub–spoke regions—identified as critical areas with crack risk in the actual product (Figure 9)—were examined in detail. After stress relief annealing, significant stress relaxation was observed, with residual stress values ranging from 27–31 MPa in the hub region and 12–23 MPa in the hub–spoke region.

When comparing the residual stress values after the handling process (Figure 10) with those remaining in the structure following the stress relief annealing process (Figure 13), an average reduction of 56.63% in the hub region and 68.62% in the hub–spoke region was observed. This clearly demonstrates the effect of the stress relief annealing process in Option #5, consistent with previous comparisons in the study of Option #5 and Option #1 in terms of both microstructure and mechanical testing, highlighting its significant impact on residual stress reduction.

## Conclusion

This study focuses on the analytical method of residual stresses in casted aluminum alloy wheels from AlSi11Mg material, both in the as-cast condition and after applied different heat treatment processes. In addition, the effects of these different heat treatment conditions on the microstructure were examined at various magnifications, specifically in the "inner flange, outer flange, and spoke" regions of the wheel. These microstructural observations were used to form preliminary predictions prior to conducting mechanical tests (namely tensile and Brinell hardness tests).

In the following stage, test specimens were extracted from the defined regions of the wheel in accordance with relevant standards and tested using universal testing machines. The tensile test results (including UTS, YS, and elongation values) as well as Brinell hardness values were obtained. These experimental outputs were compared with the earlier microstructural predictions, thereby demonstrating in detail the influence of different heat treatments.

Finally, the trial casting of wheels was modeled in the Magmasoft software with using the Magmastress module, where both production and heat treatment parameters were defined. Through this approach, the regions susceptible to residual stress-related risks were identified, and the corresponding residual stress magnitudes were calculated using the software.

As also highlighted in the literature, the presence of residual stress—particularly tensile residual stresses as identified in this study—can significantly compromise product integrity by acting as crack initiation sites during dynamic fatigue testing. Due to this critical risk, the analytically determined residual stress values obtained in this study are of substantial importance for ensuring product safety.

The main outcomes of this study can be summarized as follows:

- This study was conducted on an aluminum alloy wheel product manufactured from AlSi11Mg material using the low-pressure die casting method. In industrial production practices, AlSi7Mg and AlSi11Mg alloys are commonly preferred. However, it is well known that, due to its higher silicon content, AlSi11Mg exhibits lower heat treatability compared to AlSi7Mg. Despite this general perception, AlSi11Mg was purposely selected in this study because of its superior fluidity and mold-filling capability, and different heat treatment applications were carried out. This choice distinguishes the study from others in the literature and provides originality to the subject, specifically in the context of wheel products. One of the main reasons for selecting AlSi11Mg over its alternative (AlSi7Mg) is its considerably higher fluidity and mold-filling ability. This characteristic extends the applicability of the findings obtained from this wheel-specific investigation to other aluminum casting components—particularly those with thin sections and complex geometries—such as cylinder blocks, cylinder heads, brackets, transmission parts, and heat exchangers. Thus, the study was designed not only as an original contribution specific to wheels but also as one with potential effects for a wider range of aluminum alloy casting components.
- During the experimental studies, wheel castings were produced under industrial conditions. The chemical and mechanical tests were performed in accordance with relevant standards and using universal testing equipment, with each measurement repeated at least three times (or more) to ensure reliability.
- Similarly, during the analytical studies, the commercial Magmasoft software and its Magmastress module were run for casting simulations. In the simulation step, where the analytical solution was performed, the experimental casting and heat treatment parameters were defined identically, with the aim of obtaining final residual stress results from the software that closely approximate the actual values.

- In the microstructural analysis stage, the dendritic solidification structure was clearly observed in the as-cast specimen (Option #1), with thick dendrite arms distinctly visible. The segregation and heterogeneous structure observed in the microstructural analysis indicated low mechanical strength and hardness values, which were subsequently confirmed by tensile and hardness tests. In the specimen subjected only to artificial aging (Option #5), the dendritic structure closely looked like that of the as-cast sample; the dendrites appeared thick and sharp, while the eutectic Si morphology was observed in a coarse form. Unlike the as-cast condition, however, a limited improvement in mechanical properties was expected due to precipitation hardening, and this expectation was again validated by the mechanical tests. In the samples subjected to T6 heat treatment (Options #2, #3, and #4), the dissolution of the dendritic structure resulted in a more homogeneous microstructure. The Si particles were refined and exhibited a relatively spheroidal morphology as a result of the heat treatment. The partial dissolution of Si during solution treatment, followed by its fine and dispersed precipitation during the aging stage, contributed to the development of this microstructure. As anticipated, these samples (Options #2, #3, and #4) exhibited significantly higher mechanical properties compared to the non-T6-treated group (Options #1 and #5). Furthermore, within the T6-treated group itself, no significant differences were observed among the microstructures, leading to the expectation of similar mechanical performance, which was subsequently confirmed by the mechanical testing results.
- In the analysis of tensile and hardness values, the predictions derived from the preceding microstructural evaluations were confirmed. As indicated in the microstructural analysis, the as-cast specimens (Option #1) exhibited the lowest tensile properties (UTS, YS, and elongation) as well as the lowest hardness values. In the specimens subjected only to artificial aging (Option #5), a limited improvement was observed due to restricted precipitation hardening within the structure. When these two conditions (Option #1 and Option #5) were compared, Option #5 demonstrated a relatively modest enhancement—approximately 6% on average across the defined wheel regions—compared to the as-cast condition.
- In the specimens subjected to T6 heat treatment (Options #2, #3, and #4), a pronounced improvement was observed because of the treatment. Specifically for the wheel product, a significant increase was noted in the flange regions, whereas relatively lower values were obtained in the spoke region. This difference is attributed to the slower cooling rate of the spoke region compared to the flanges. These regional variations, however, corresponded to a limited difference of approximately 5–6% in terms of average values. Among all groups, the T6-treated specimens (Options #2, #3, and #4) clearly exhibited the highest UTS, YS, and elongation results. Particularly in terms of UTS and YS, Option #2 (150 min artificial aging) and Option #3 (120 min artificial aging) showed nearly identical values. Taking into account the corresponding hardness values, Option #3 emerged as the most favorable among the different conditions. Within the T6-treated group, the lowest tensile test results (UTS and YS) were obtained for Option #4. Based on these findings, a minimum artificial aging time of 120 minutes, as in Option #3, is recommended to achieve the most favorable combination of mechanical properties and hardness. At shorter aging durations (Option #4, 90 min), reductions of 5–6% in UTS and 7–9% in YS were observed across different wheel regions. Conversely, extending the aging duration to 150 minutes (Option #2) did not yield significant improvements and resulted only in marginal increases.
- When evaluating the simulation results, the first analysis was performed for Option #1, also referred to as the as-cast condition. Although this option did not undergo any heat treatment, it was exposed to thermal effects induced by the production handling process, resulting in an average residual stress of 68.97 MPa in the critical hub region (Figure 9) as shown in Figure 10. The second set of analyses focused on T6 heat-treated options, specifically examining the specimens with the longest (Option #2) and shortest (Option #4) artificial aging durations. After the first step of the T6 process, the solution treatment, residual stresses in the structure were nearly zero. Maximum residual stresses occurred after the quenching step, while in the final step—the artificial aging process—Option #2, with the longer aging duration, exhibited an average residual stress of 107.49 MPa in the critical hub region (Figure 11). For Option #4, with the shorter aging duration, the corresponding average residual stress in the same region was 110.57 MPa (Figure 12). These results indicate that longer artificial aging provides a 5.5% improvement in the critical hub region. Due to the minimal differences between Options #2 and #4, it was anticipated that Option #3 would give intermediate values with negligible variation, and therefore, a separate analysis for Option #3 was considered unnecessary. Finally, in the analysis of Option #5, the effect of the stress relief annealing process was investigated. Comparison

of the residual stress after the handling process (Figure 10) with those following stress relief annealing clearly shows a significant reduction. After this step, the residual stress in the critical hub region decreased by 56.63%, demonstrating the substantial effect of the stress relief annealing process.

Suggestions for future work:

- The findings of the present study, which are based on simulation results, may be validated using destructive methods (such as the hole-drilling method) or non-destructive techniques (such as the XRD method). In this way, comparing the results obtained from the analytical approach employed in this study with those derived from destructive or non-destructive methods could constitute a valuable investigation for identifying and analyzing potential discrepancies.
- By introducing Mg additions to the existing chemical composition—while remaining within the compositional limits of AlSi11Mg—the formation of $Mg_2Si$ phases during the heat treatment process may be promoted, enabling investigations on alternative materials with enhanced mechanical properties.
- The water quenching conditions employed in this study (80 °C ± 5 °C) may be extended to include different cooling media and temperatures—such as air cooling, polymer-based water quenching, and oil quenching—in order to investigate the influence of the quenching medium on residual stresses.

## Acknowledgment

The authors would like to thank Dokuz Eylül University and DöktaşDökümcülük Tic. ve San. A.Ş for their continued support. The sample support provided by Döktaş Dökümcülük Tic. ve San. A.Ş is also appreciated.

## Funding

Open access funding provided by the Scientific and Technological Research Council of Türkiye (TÜBITAK).

**Conflict of interest** The authors have no conflicts of interest to declare that are relevant to the content of this article.

**Open Access** This article is licensed under a Creative Commons Attribution 4.0 International License, which permits use, sharing, adaptation, distribution and reproduction in any medium or format, as long as you give appropriate credit to the original author(s) and the source, provide a link to the Creative Commons licence, and indicate if changes were made. The images or other third party material in this article are included in the article's Creative Commons licence, unless indicated otherwise in a credit line to the material. If material is not included in the article's Creative Commons licence and your intended use is not permitted by statutory regulation or exceeds the permitted use, you will need to obtain permission directly from the copyright holder. To view a copy of this licence, visit http://creativecommons.org/licenses/by/4.0/.

## REFERENCES

1. Dispinar, D. Determination of Metal Quality of Aluminium and Its Alloys (PhD Thesis). School of Metallurgy and Materials – The University of Birmingham. 1-4 (2005).
2. European Aluminium (2023a), Aluminium: A Unique Metal Driving the Green Transition Accessed 29.09.2025
3. C. Karabulut, G. Malkoç, A.Y. Kaya et al., Influence of different Fe levels on mechanical properties of AlSi7Mg0.3 aluminum casting alloys. Inter Metalcast **18**, 3081–3094 (2024). https://doi.org/10.1007/s40962-023-01227-y
4. A. Tabatabaeian, A.R. Ghasemi, M.M. Shokrieh, B. Marzbanrad, M. Baraheni, M. Fotouhi, Residual stress in engineering materials: a review. Adv. Eng. Mater. (2022). https://doi.org/10.1002/adem.202100786
5. H. Alipooramirabad, S. Kianfar, A. Paradowska et al., Residual stress measurement in engine block—an overview. Int. J. Adv. Manuf. Technol. **131**, 1–27 (2024). https://doi.org/10.1007/s00170-024-13071-3
6. E. Carrera, A. Rodríguez, J. Talamantes, S. Valtierra, R. Colás, Measurement of residual stresses in cast aluminium engine blocks. J. Mater. Process. Technol. **189**(1–3), 206–210 (2007). https://doi.org/10.1016/j.jmatprotec.2007.01.023
7. N.S. Rossini, M. Dassisti, K.Y. Benyounis, A.G. Olabi, Methods of measuring residual stresses in components. Mater. Des. **35**, 572–588 (2012). https://doi.org/10.1016/j.matdes.2011.08.022
8. Campbell, J., Complete Casting Handbook: Metal Casting Processes, Metallurgy, Techniques and Design (Elsevier, 2015).
9. Kaufman, J.G., Introduction to Aluminum Alloys and Tempers (ASM International, Materials Park, OH, 2000).
10. M. Beder, S.B. Akçay, T. Varol et al., The effect of heat treatment on the mechanical properties and oxidation resistance of AlSi10Mg alloy. Arab. J. Sci. Eng. **49**, 15335–15346 (2024). https://doi.org/10.1007/s13369-024-08971-1
11. Rheinfelden Alloys, primary aluminium casting alloys, datasheet (Aluminium Rheinfelden GmbH) handbook-primary-aluminium-casting-alloys_RHEINFELDEN-ALLOYS_2016_EN.pdf Accessed 29.09.2025
12. A. Jarco, Effect of soft annealing treatment on impact strength and hardness of the en AC-Alsi11 alloy. Arch. Foundry Eng. **17**(3), 55–58 (2017). https://doi.org/10.1515/afe-2017-0090

13. A. Jarco, J. Pezda, Effect of heat treatment process and optimization of its parameters on mechanical properties and microstructure of the AlSi11(Fe) alloy. Materials **14**(9), 2391 (2021). https://doi.org/10.3390/ma14092391
14. D. Vuksanović, V. Asanović, J. Šćepanović, D. Radonjić, Effect of chemical composition and T6 heat treatment on the mechanical properties and fracture behaviour of Al-si alloys for Ic engine components. J. Min. Metall.Sect. B. **57**(2), 195–207 (2021). https://doi.org/10.2298/JMMB190510014V
15. L. Pedersen, L. Arnberg, The effect of solution heat treatment and quenching rates on mechanical properties and microstructures in AlSiMg foundry alloys. Metall. Mater. Trans. A **32A**, 525–532 (2001)
16. M.H. Abdelaziz, A.M. Samuel, H.W. Doty, S. Valtierra, F.H. Samuel, Effect of additives on the microstructure and tensile properties of Al-Si alloys. J. Mater. Res. Technol. **8**(2), 2255–2268 (2019). https://doi.org/10.1016/j.jmrt.2019.03.003
17. Altınel, A.İ. The mechanical properties of Some cast aluminium alloys (Sr modified AlSi11Mg) (M.Sc. Thesis) Dokuz Eylül University, Graduate School of Natural and Applied Sciences, Mechanical Engineering, Material Science Program, June 1999.
18. M. Neuser, O. Grydin, Y. Frolov et al., Influence of solidification rates and heat treatment on the mechanical performance and joinability of the cast aluminium alloy AlSi10Mg. Prod. Eng. Res. Devel. **16**, 193–202 (2022). https://doi.org/10.1007/s11740-022-01106-1
19. Menteşe, E.B., Aydoğan, F., Saklakoğlu, N., Alsi10mg Alaşımlı Döküm Parçalar İçin Isıl İşlem Prosesinde Optimizasyon Çalışmaları 2nd National Foundry Congress, İzmir, 223–231 (2019).
20. E.M. Johnson, T.R. Watkins, J.E. Schmidlin et al., A benchmark study on casting residual stress. Metall. Mater. Trans. A **43**, 1487–1496 (2012). https://doi.org/10.1007/s11661-011-0907-5
21. Menne, R.J., Weiss, U., Brohmer, A., Egner-Walter, A., Weber, M., Oelling, P. Implementation of Casting Simulation for Increased Engine Performance and Reduced Development Time and Costs – Selected Examples from FORD R&D Engine Projects 28th International Vienna Engine Symposium, Vienna, (2007).
22. A. Long, D. Thornhill, C. Armstrong et al., Stress correlation between instrumentation and simulation analysis of the die for high pressure die casting. Inter Metalcast **7**, 27–41 (2013). https://doi.org/10.1007/BF03355551
23. Q. Jiang, Z. Zhao, Z. Xu, J. Sun, X. Chen, B. Su, Z. Zhao, W. Jiang, Effect of Residual Stresses on Wheel Fatigue Life and Experimental Validation. Machines **10**(10), 924 (2022). https://doi.org/10.3390/machines10100924
24. Y. He, J. Liu, X. Yu et al., Performance enhancing of large aluminum alloy wheels through coupled solidification-fatigue stress simulation. Inter Metalcast **19**, 3328–3342 (2025). https://doi.org/10.1007/s40962-024-01505-3
25. Heger, J., Hartmann, G., Bodenburg, M. Integration of manufacturing aspects into the development of heavy-duty engine cast components 225–237 (2019). https://doi.org/10.1007/978-3-658-25889-4_14
26. P. Li, D.M. Maijer, T.C. Lindley, P.D. Lee, A through process model of the impact of in-service loading, residual stress, and microstructure on the final fatigue life of an A356 automotive wheel. Mater. Sci. Eng. A **460**, 20–30 (2007). https://doi.org/10.1016/j.msea.2007.01.076
27. P. Li, D.M. Maijer, T.C. Lindley et al., Simulating the residual stress in an A356 automotive wheel and its impact on fatigue life. Metall. Mater. Trans. B **38**, 505–515 (2007). https://doi.org/10.1007/s11663-007-9050-5
28. Z. Cai, P. Mayr, R. Fernandez et al., Residual stress determination of cast aluminium benchmark components using strain relief techniques. Exp. Mech. **64**, 441–452 (2024). https://doi.org/10.1007/s11340-024-01033-5
29. A. Özel, S. Şen, M. Belevi, Effects of residual stresses caused by different types of loading on silent chain strength. J. Eng. Environ. Sci. **22**, 461–470 (1998)
30. M. Kreins, M. Hippe, F. Funken et al., Effect of shrinkage versus hydrogen pores on fatigue life of cast AlSi11Mg alloy. Inter Metalcast **19**, 109–128 (2025). https://doi.org/10.1007/s40962-024-01288-7
31. M.A.A. Khan, A.K. Sheikh, A comparative study of simulation software for modelling metal casting processes. Int. J. Simul. Model. **17**(2), 197–209 (2018). https://doi.org/10.2507/IJSIMM17(2)402
32. O. Özaydın, A. Dikicioğlu, Product development of alternative alloy wheel material with improved mechanical properties. Inter Metalcast **17**, 2085–2102 (2023). https://doi.org/10.1007/s40962-022-00914-6
33. U. Kutsal, Y. Arslan, O. Ozaydin et al., Heat treatment simulation of aluminum alloy wheels and investigation of process steps. Inter Metalcast **18**, 1556–1572 (2024). https://doi.org/10.1007/s40962-023-01132-4
34. R. Jha, G.S. Dulikravich, Solidification and heat treatment simulation for aluminum alloys with scandium addition through CALPHAD approach. Comput. Mater. Sci. (2020). https://doi.org/10.1016/j.commatsci.2020.109749
35. Kandil, F. A., Lord, J. D., Fry, A. T., Grant, P. v. A Review of Residual Stress Measurement Methods-A Guide to Technique Selection. NPL Report MATC(A)04, National Physical Laboratory, Teddington, UK (2001).
36. J. Guo, H. Fu, B. Pan, R. Kang, Recent progress of residual stress measurement methods: a review. Chin.

J. Aeronaut. **34**(2), 54–78 (2021). https://doi.org/10.1016/j.cja.2019.10.010
37. X. Li, J. Liu, H. Wu, K. Miao, H. Wu, R. Li, C. Liu, W. Fang, G. Fan, Research progress of residual stress measurement methods. Heliyon (2024). https://doi.org/10.1016/j.heliyon.2024.e28348
38. J.S. Robinson, W. Redington, The influence of alloy composition on residual stresses in heat treated aluminium alloys. Mater Charact **105**, 47–55 (2015). https://doi.org/10.1016/j.matchar.2015.04.017
39. J.E. Wyatt, J.T. Berry, A.R. Williams, Residual stresses in aluminum castings. J. Mater. Process. Technol. **191**(1–3), 170–173 (2007). https://doi.org/10.1016/j.jmatprotec.2007.03.018
40. Özaydın, O. Alternatif Alaşımlı Jant Malzemesi İle Mekanik Özellikleri İyileştirilmiş Ürün Geliştirilmesi (M.Sc. Thesis) Istanbul Technical University, Graduate School of Science and Engineering, Department of Mechanical Engineering, Materials and Manufacturing Program, June 2019.

**Publisher's Note** Springer Nature remains neutral with regard to jurisdictional claims in published maps and institutional affiliations.